

Topographically-induced enstrophy production/dissipation in coastal models

E. Terrile

D. I. Am., University of Genoa, Via Montallegro 1, 16145 Genoa, Italy

R. Briganti

D. S. I. C., University of "Roma Tre," Via Vito Volterra 62, 00146 Rome, Italy

M. Brocchini^{a)}

D. I. Am., University of Genoa, Via Montallegro 1, 16145 Genoa, Italy

J. T. Kirby

Center for Applied Coastal Research, University of Delaware, Newark, Delaware 19716

(Received 24 January 2006; accepted 19 October 2006; published online 26 December 2006)

Vorticity and enstrophy production and dissipation are studied for both wave-averaged and wave-resolving (Boussinesq-type) models of wave-induced near shore circulation. Quadratic flow properties of fundamental importance for shallow-water turbulence, i.e., energy and enstrophy, whose sources/sinks are clearly identifiable by positive/negative-definite contributions in the appropriate transport equations, are taken as the most suitable indicators for assessing model performance in describing flows characterized by large-scale vortices. Two state-of-the-art models, SHORECIRC and FUNWAVE2D, have been evaluated in detail. Suitable transport equations for enstrophy are derived and analyzed to get a clear insight into the mechanisms of generation/dissipation of this quantity in both models. Analytical results show that steep gradients of the total flow depth act as sinks as well as sources for vorticity and enstrophy, similar to the results of Brocchini and Colombini [M. Brocchini and M. Colombini, *Phys. Fluids* **16**, 2469 (2004)]. Predictive estimates have been given for the rate of change of circulation for waves breaking over a bar or breakwater and the vorticity source and sink terms have been numerically analyzed. The comparison between numerical results obtained using the two different circulation models reveals that while wave-resolving computations give well-structured rip currents, the wave-averaged model predicts less organized flows, given the different structure of the circulation forcing terms. The analysis of equivalent enstrophy-forcing terms characterizing the two models shows that they are all proportional to depth gradients in the case of wave-resolving models while their intensity is mainly due to the gradients of the wave-induced velocity for wave-averaged models. Energetic considerations are also given in support of the proposed vorticity/enstrophy generation mechanisms. Wave-averaged computations clearly show that, apart from bottom friction, the most intense dissipation mechanism is due to classic viscous effects $[-\nu_T(\nabla\tilde{\omega})^2]$ while depth gradients weakly contribute. Rather surprisingly this also occurs for the wave-resolving model. © 2006 American Institute of Physics. [DOI: 10.1063/1.2400076]

I. INTRODUCTION

It is well known that differential wave breaking, especially when occurring over submerged bars or breakwaters, can generate vorticity in the form of macrovortices (e.g., Peregrine^{2,3} and Bühler⁴) i.e., vertical eddies with horizontal size larger than the flow depth. These macrovortices play a major role in the horizontal flow mixing; therefore their production/dissipation and evolution are very important for the study of coastal zone hydrodynamics and of induced mixing (Piattella *et al.*⁵).

Analytical studies of breaking-wave-generated macrovortices have shown behaviors which are mainly dependent on the local topographies; see Brocchini *et al.*⁶ and Kennedy

*et al.*⁷ Such studies lead to a better understanding of the main mechanisms describing the generation/evolution of macrovortices. However, to get clearer and quantitative descriptions of macrovortex evolution, and in general of vorticity patterns, numerical simulations of near shore flows are needed.

Two classes of near shore circulation models can be used for this purpose: wave-averaged and wave-resolving models. Wave-averaged models are currently very popular for the study of near shore circulation patterns. In particular SHORECIRC, developed by the Center for Applied Coastal Research (CACR) of the University of Delaware, provides useful solutions for a number of coastal circulations systems (e.g., Putrevu and Svendsen⁸ and Svendsen *et al.*⁹). On the other hand, wave-resolving models can be used as circulation models provided they preserve a correct description of the wave-current interactions. Models based on Boussinesq-type

^{a)}Present address: Istituto di Idraulica e Infrastrutture Viarie, Università Politecnica della Marche, 60131 Ancona, Italy.

equations such as FUNWAVE2D (also developed at CACR) can describe the features of near shore circulation patterns like rip currents and long shore currents, as shown in Chen *et al.*^{10,11}

Haas and Svendsen¹² were the first to give predictions of topographically-generated vorticity in the presence of rip channels using SHORECIRC. This study illustrated the transition of the flow towards instability as well as the role of wave-current interactions in the evolution of the circulation patterns. A description of the vorticity and enstrophy equations associated with the SHORECIRC momentum equations has been given in Zhao *et al.*¹³ These studies illustrate some of the main characteristics of the vorticity patterns as described by the model but they do not quantify the contribution of the source and sink terms to the generation and dissipation of enstrophy and vorticity.

Detailed numerical simulations of rip currents using a Boussinesq-type model have been carried out by Chen *et al.*¹⁰ in which a description of the flow instability is also given. After deriving the vorticity equation associated with the specific set of Boussinesq-type equations, they discussed the role of wave breaking terms as vorticity sources. Although Haas and Svendsen¹² and Chen *et al.*^{10,11} use the same configuration for the tested rip channel, no direct comparison between the amount of generation/dissipation of vorticity/enstrophy predicted by the two approaches has been given as yet. However, recent work by Kirby *et al.*¹⁴ has shown that wave-averaged circulation models and wave-resolving Boussinesq-type models can induce very different vorticity dynamics, and, in turn, near shore circulation patterns, even when the models are configured similarly and applied to the same field cases. Hence, a direct comparison on a common experimental flow configuration may shed light on various differences in the solutions given by the two different approaches. Moreover the existing literature does not report any test case of both models working with a similar, if not identical, set of input parameters.

It is, finally, recognized that circulation models of shallow oceanic/atmospheric flows where mesoscale eddies are permitted, must carefully reproduce both energy and enstrophy cascading, hence allowing for simulations that faithfully represent the rich variety of observed flow regimes.^{15,16} Similar analyses should be performed to assess the value of near shore circulation models in reproducing macrovortex-dominated dynamics, also using available experimental data (e.g., Piattella *et al.*⁵), and bearing in mind that fundamental is the identification of sources/sinks of enstrophy which force the cascading process.

These considerations are the starting point of our contribution. Among the several, interesting, aspects of this comparison we chose to focus on the generation/dissipation mechanisms of vorticity/enstrophy in the predicted flows as described by the equations of SHORECIRC and FUNWAVE2D. With an approach conceptually similar to that used when stating the *Theorem for the Mechanical Power* (e.g., Aris,¹⁷ pp. 120–123 and Batchelor,¹⁸ pp. 151–156) we inspect how the models describe the rotational properties of the flow. In other words, the enstrophy, quadratic flow properties of fundamental importance for

shallow-water turbulence,^{19,20} whose sources/sinks are clearly identifiable by positive/negative-definite contributions in the appropriate transport equation, is taken, with energy, as the fundamental indicator for assessing the model performances in describing flows characterized by large-scale vortices. Hence, suitable enstrophy equations are first derived starting from the models equations (Sec. II). Subsequently positive-definite and negative-definite terms, i.e., those contributions which act as sources or sinks of enstrophy, are highlighted. Although this process leads to formally complex equations, it is the only method to properly separate the production/dissipation contributions. Once these terms are isolated and physically described, it is possible to study their spatial structure and magnitude. Although various analyses of vorticity dynamics reproduced by coastal circulation models are available (Chen *et al.*^{10,11} and Zhao *et al.*¹³) we know of no study, apart from that of Brocchini and Colombini¹ (hereafter BC04), which has ever focused on detailing the specific rate of each contribution to the vorticity/enstrophy equations. This is the main aim of the present work along with an illustration of specific, related, flow features. In more detail the productive and dissipative terms are identified studying the terms describing “wave-wave,” “wave-current” and “current-current” interactions. The dimensional forms of the equations have been used as the most suitable to compare two largely different models like SHORECIRC and FUNWAVE2D, the aim being that of inspecting features of similar mechanisms (e.g., wave-breaking production, viscous dissipation, topographic forcing, wave-wave interaction, etc.) in the two models rather than detailing the influence of nonlinear and dispersive terms (these contributing, at various orders, to each of the mentioned physical mechanisms). It is also clear that no exact quantitative comparison between the two models is sought, for which potential vorticity and enstrophy would probably be more suitable (see Appendices B and D), the scope being mainly that of a minute inspection of the physical mechanism impossible to achieve through the potential vorticity which, by definition, introduces “hidden terms.” Together with a decomposition of the various terms of the vorticity and enstrophy equations, numerical simulations have been performed. The detailed role of the topography is investigated on the basis of numerical computations carried out with a typical “rip-current topography” (Sec. III). A detailed description of the energy dissipation mechanisms is given in Sec. IV, while Sec. V rounds up the paper.

II. THEORETICAL ANALYSIS

Here we analyze in detail the vorticity and the enstrophy equations obtained for both types of circulation models. The equations considered are those implemented in the wave-averaged model SHORECIRC and the wave-resolving model FUNWAVE2D.

A. The wave-averaged circulation model

In the wave-averaged circulation model SHORECIRC the instantaneous horizontal velocity $u_i(x, y, z, t)$, after turbulence averaging, which implies that the generic turbulent component satisfies $\langle u' \rangle = 0$, is split in two components (Putrevu and Svendsen⁸) to distinguish waves from the mean flow,

$$u_i(x, y, z, t) = u_{wi}(x, y, z, t) + V_i(x, y, z, t) \quad (1)$$

where x and y are, respectively, the cross shore and long shore coordinates [with indices $i(j)=1, 2$], while z is the vertical coordinate. u_w is the generic wave component, defined so that its time average over the wave period below the trough level satisfies $\bar{u}_{wi}=0$, and V_i is the generic current component. The time-averaged and depth-integrated equations of mass conservation and momentum have been derived for nonuniform currents over the variable depth.

Representing the mean surface elevation with $\bar{\zeta}$ and the still water depth with h_0 , the local water depth h is

$$h = h_0 + \bar{\zeta}. \quad (2)$$

After some manipulation and using the analysis reported in Appendix A, the depth-integrated, short-wave-averaged governing equations

$$\bar{\zeta}_{,t} + \nabla \cdot (h \tilde{\mathbf{V}}) = 0, \quad (3)$$

$$\begin{aligned} \tilde{\mathbf{V}}_{,t} + (\tilde{\mathbf{V}} \cdot \nabla) \tilde{\mathbf{V}} = & -g \nabla \bar{\zeta} - \frac{1}{\rho h} \nabla \cdot (\mathbf{S} - \mathbf{T} + \mathbf{L}) - \frac{1}{\rho h} \boldsymbol{\tau}^B \\ & + \frac{1}{\rho h} \boldsymbol{\tau}^S, \end{aligned} \quad (4)$$

where g is the gravity acceleration, $\tilde{\mathbf{V}} = (\tilde{U}, \tilde{V}, 0)$ is the depth-uniform velocity vector, given by Eq. (A8), \mathbf{S} , \mathbf{L} , and \mathbf{T} are, respectively, the radiation stress tensor, given by Eq. (A11), the dispersive mixing tensor, given by Eq. (A12) and representing the contribution from the depth-varying currents, the quasi-3D dispersive term, and the turbulent stress tensor,

given by Eq. (A13), while $\boldsymbol{\tau}^B$ and $\boldsymbol{\tau}^S$ are the bottom and surface shear stresses.

The vorticity equation is found by taking the curl of the momentum equation (4)

$$\begin{aligned} \nabla \times \tilde{\mathbf{V}}_{,t} + \nabla \times (\tilde{\mathbf{V}} \cdot \nabla) \tilde{\mathbf{V}} \\ = & -\frac{1}{\rho} \nabla \times \left[\frac{1}{h} \nabla \cdot (\mathbf{S} - \mathbf{T} + \mathbf{L}) \right] \\ & + \frac{1}{\rho} \nabla \times \left[\frac{1}{h} (\boldsymbol{\tau}^S - \boldsymbol{\tau}^B) \right]. \end{aligned} \quad (5)$$

Defining the depth-averaged vertical vorticity related to $\tilde{\mathbf{V}}$ as

$$\tilde{\boldsymbol{\Omega}} \equiv \hat{\mathbf{k}} \tilde{\omega} = \hat{\mathbf{k}} (\tilde{V}_{,x} - \tilde{U}_{,y}), \quad (6)$$

we can write the vorticity equation as

$$\begin{aligned} \frac{D\tilde{\omega}}{Dt} + \tilde{\omega} \nabla \cdot \tilde{\mathbf{V}} = & -\frac{1}{\rho} \hat{\mathbf{k}} \cdot \left\{ \nabla \times \left[\frac{1}{h} \nabla \cdot (\mathbf{S} - \mathbf{T} + \mathbf{L}) \right] \right\} \\ & + \frac{1}{\rho} \hat{\mathbf{k}} \cdot \left\{ \nabla \times \left[\frac{1}{h} (\boldsymbol{\tau}^S - \boldsymbol{\tau}^B) \right] \right\}. \end{aligned} \quad (7)$$

A detailed term-by-term examination of Eq. (7) is given in Appendix A. The final form of the vorticity equation appears as in Eq. (A37), where the effective viscosity ν_T can be a function of the flow and, in turn, of the spatial coordinates. This effective viscosity is used to account for, through a Fickian-type approach, all momentum mixing contributions due to both small-scale horizontal turbulence and the dispersion introduced by vertical gradients of the horizontal flow (e.g., BC04).

From the vorticity equation (A37), the transport equation for the enstrophy ($\tilde{\omega}^2$) can be easily derived. The viscous terms are here manipulated, as standard when identifying purely dissipative contributions (e.g., BC04), with the specific aim of highlighting the presence of always negative terms: standard diffusive-type terms appearing in (A37) lead, in Eq. (8), to both dissipative terms (e.g., $T.I$) and flux-type terms [e.g., $\nu_T \nabla \cdot (\tilde{\omega} \nabla \tilde{\omega})$]. The enstrophy equation, obtained by taking the curl of (7), is given by

$$\begin{aligned} \frac{1}{2} \frac{D\tilde{\omega}^2}{Dt} + \tilde{\omega}^2 \nabla \cdot \tilde{\mathbf{V}} = & S.I + S.II + S.III + S.IV + CC + WC + \nu_T \nabla \cdot (\tilde{\omega} \nabla \tilde{\omega}) \\ & - \underbrace{\nu_T (\nabla \tilde{\omega})^2}_{(T.I)} + \tilde{\omega} \nabla \nu_T \cdot \nabla \tilde{\omega} - \underbrace{\frac{\nu_T \tilde{\omega}}{h} \hat{\mathbf{k}} \cdot [\nabla \times (\nabla h \times \hat{\mathbf{k}} \tilde{\omega})]}_{(T.II)} + \underbrace{\frac{\nu_T \tilde{\omega}}{h} \hat{\mathbf{k}} \cdot \left[\frac{\nabla h}{h} \times (\nabla h \times \hat{\mathbf{k}} \tilde{\omega}) \right]}_{(T.III)} \\ & + 2\tilde{\omega} \hat{\mathbf{k}} \cdot (\nabla \nu_T \times \nabla^2 \tilde{\mathbf{V}}) + \frac{\tilde{\omega} \nu_T}{h} \hat{\mathbf{k}} \cdot \left[\left(\nabla - \frac{\nabla h}{h} \right) \times (2 \nabla h \cdot \nabla \tilde{\mathbf{V}}) \right] + \frac{\tilde{\omega}}{h} \hat{\mathbf{k}} \cdot [\nabla \nu_T \times (2 \nabla h \cdot \nabla \tilde{\mathbf{V}} - \nabla h \times \hat{\mathbf{k}} \tilde{\omega})] \\ & + \tilde{\omega} \hat{\mathbf{k}} \cdot [\nabla \times (2 \nabla \nu_T \cdot \nabla \tilde{\mathbf{V}} - \nabla \nu_T \times \hat{\mathbf{k}} \tilde{\omega})] - \tilde{\omega} \hat{\mathbf{k}} \cdot \left\{ \nabla \times \left[\frac{1}{h} \boldsymbol{\tau}^B \right] \right\} \end{aligned} \quad (8)$$

where $S.I$, $S.II$, $S.III$, and $S.IV$ represent short-wave contributions to the enstrophy dynamics and are defined as

$$\begin{aligned}
 S.I &= -\hat{\mathbf{k}} \cdot \overline{\int_{-h_0}^{\zeta} \frac{1}{h} [\tilde{\omega} (\nabla (\nabla \cdot \mathbf{u}_w) \times \mathbf{u}_w)] dz} - \overline{\tilde{\omega} \hat{\mathbf{k}} \cdot \left\{ \nabla \times \left[\frac{1}{h} [\nabla \zeta \cdot \mathbf{G}_w] \right] + \frac{1}{h} [\nabla \zeta \times (\nabla \cdot \mathbf{G}_w)] \right\}}_{\zeta} \\
 &\quad - \overline{\tilde{\omega} \hat{\mathbf{k}} \cdot \left\{ \nabla \times \left[\frac{1}{h} [\nabla h_0 \cdot \mathbf{G}_w] \right] + \frac{1}{h} [\nabla h_0 \times (\nabla \cdot \mathbf{G}_w)] \right\}}_{-h_0}, \\
 S.II &= \overline{\int_{-h_0}^{\zeta} \frac{1}{h} (\mathbf{u}_w \cdot \tilde{\omega} \nabla \omega_w) dz}, \quad S.III = \overline{\int_{-h_0}^{\zeta} \frac{1}{h} (2\tilde{\omega} \omega_w \nabla \cdot \mathbf{u}_w) dz}, \quad (9)
 \end{aligned}$$

$$S.IV = \hat{\mathbf{k}} \cdot \overline{\int_{-h_0}^{\zeta} \left[\tilde{\omega} (\nabla \cdot \mathbf{u}_w) \left(\frac{\nabla h}{h^2} \times \mathbf{u}_w \right) + \tilde{\omega} \frac{\nabla h}{h^2} \times (\mathbf{u}_w \cdot \nabla \mathbf{u}_w) \right] dz} + \overline{\int_{-h_0}^{\zeta} \tilde{\omega} \omega_w \left(\mathbf{u}_w \cdot \frac{\nabla h}{h^2} \right) dz},$$

where \mathbf{G}_w is given in Appendix A.

In keeping with the fact that the wave driver used in SHORECIRC uses a framework based on a slowly modulated plane wave to represent wave properties, the radiation stress-based terms $S.I$ – $S.IV$ can be represented approximately by

$$\begin{aligned}
 S.I &\approx \hat{\mathbf{k}} \cdot \left\{ \frac{1}{h} \nabla \times \nabla \cdot \mathbf{S} \right\} - (S.II + S.III), \\
 S.II &\approx -\frac{\tilde{\omega}}{h} \nabla \hat{\omega} \cdot \mathbf{Q}_w, \\
 S.III &\approx -\frac{2\tilde{\omega}\hat{\omega}}{h} \nabla \cdot \mathbf{Q}_w, \quad S.IV \approx \hat{\mathbf{k}} \cdot \left\{ \nabla \frac{1}{h} \times \nabla \cdot \mathbf{S} \right\},
 \end{aligned}$$

where \mathbf{Q}_w is the wave-induced volume flux given by Eq. (A6).

Terms CC and WC are, respectively, the current-current and the wave-current contributions to the enstrophy dynamics, and are defined as

$$\begin{aligned}
 CC &= -\int_{-h_0}^{\bar{\zeta}} \frac{1}{h} (\tilde{\omega} \hat{\mathbf{k}} \cdot [\nabla (\nabla \cdot \mathbf{V}_1) \times \mathbf{V}_1] + \mathbf{V}_1 \cdot \tilde{\omega} \nabla \omega_1 + 2\tilde{\omega} \omega_1 \nabla \cdot \mathbf{V}_1) dz - \overline{\tilde{\omega} \hat{\mathbf{k}} \cdot \left\{ \nabla \times \left[\frac{1}{h} [\nabla \bar{\zeta} \cdot \mathbf{G}_1] \right] + \frac{1}{h} [\nabla \bar{\zeta} \times (\nabla \cdot \mathbf{G}_1)] \right\}}_{\bar{\zeta}} \\
 &\quad - \overline{\tilde{\omega} \hat{\mathbf{k}} \cdot \left\{ \nabla \times \left[\frac{1}{h} [\nabla h_0 \cdot \mathbf{G}_1] \right] + \frac{1}{h} [\nabla h_0 \times (\nabla \cdot \mathbf{G}_1)] \right\}}_{-h_0} - \hat{\mathbf{k}} \cdot \int_{-h_0}^{\bar{\zeta}} \left[\tilde{\omega} (\nabla \cdot \mathbf{V}_1) \left(\nabla \frac{1}{h} \times \mathbf{V}_1 \right) + \tilde{\omega} \nabla \frac{1}{h} \times (\mathbf{V}_1 \cdot \nabla \mathbf{V}_1) \right] dz \\
 &\quad - \int_{-h_0}^{\bar{\zeta}} \tilde{\omega} \omega_1 \left(\mathbf{V}_1 \cdot \nabla \frac{1}{h} \right) dz, \quad (10)
 \end{aligned}$$

$$\begin{aligned}
WC = & +2\tilde{\omega}\hat{\mathbf{k}} \cdot \left\{ \hat{\mathbf{V}} \times \left[\nabla \times \left(\hat{\mathbf{V}} \times \frac{\nabla h}{h} \right) \right] - \hat{\mathbf{V}} \right. \\
& \times \left(\frac{\nabla h}{h} \cdot \nabla \hat{\mathbf{V}} \right) + \hat{\mathbf{V}} \times \left(\frac{\nabla h}{h} \cdot \hat{\Omega} \right) \left. \right\} + 2\tilde{\omega}\hat{\omega} \left(\hat{\mathbf{V}} \cdot \frac{\nabla h}{h} \right) \\
& + 2\tilde{\omega}\hat{\mathbf{k}} \cdot \left[\hat{\mathbf{V}} \times \nabla(\nabla \cdot \hat{\mathbf{V}}) \right] + 2\hat{\mathbf{V}} \cdot \tilde{\omega} \nabla \hat{\omega} \\
& + 4\tilde{\omega}\hat{\omega} \nabla \cdot \hat{\mathbf{V}}, \tag{11}
\end{aligned}$$

where \mathbf{V}_1 represents the depth-varying part of the velocity as defined in (A7) and $\hat{\mathbf{V}}$ is given by (A29), while ω_1 and $\hat{\omega}$ are, respectively, their related vorticity variables.

In SHORECIRC, as shown in Appendix A, the WC term is approximated through Eqs. (A28)–(A30). Here all the terms given by the portion of the velocity vector variable with the depth (\mathbf{V}_1) are set to zero since the comparison with FUNWAVE2D requires to consider only the depth-uniform velocity contribution.

Of particular interest are the T -terms, where ($T.I$) represents the most classic contribution to the enstrophy dissipation due to viscous effects, while the role of ($T.II$) and ($T.III$) in the enstrophy budget is better highlighted by the following manipulation:

$$\begin{aligned}
(T.II) = & -\frac{\nu_T \tilde{\omega} \hat{\mathbf{k}}}{h} \cdot \left[\nabla \times (\nabla h \times \hat{\mathbf{k}} \tilde{\omega}) \right] \\
= & \frac{\nu_T}{h} \left[\underbrace{\frac{1}{2} \nabla \tilde{\omega}^2 \cdot \nabla h}_{(T.IIa)} + \underbrace{\tilde{\omega}^2 \nabla^2 h}_{(T.IIb)} \right] \tag{12}
\end{aligned}$$

$$(T.III) = \frac{\nu_T \tilde{\omega} \hat{\mathbf{k}}}{h} \cdot \left[\frac{\nabla h}{h} \times (\nabla h \times \hat{\mathbf{k}} \tilde{\omega}) \right] = -\nu_T \left(\frac{\tilde{\omega} \nabla h}{h} \right)^2. \tag{13}$$

Although term ($T.II$), as a whole, is not positive or negative definite, it is easy to recognize in term ($T.IIa$) one of the production terms of Schär and Smith,²¹ who used a viscous shallow-water approach to investigate topographically-forced shallow vortical flows. Furthermore in typical coastal applications, i.e., for monotonically upward-concave beach profile, the contribution of ($T.IIb$) is negative (BC04). Finally, Eq. (13) clearly shows that ($T.III$), is always negative, and represents a sink term for the enstrophy balance.

B. The wave-resolving model

The extended Boussinesq-type equations of both Nwogu²² and Wei *et al.*²³ (hereinafter WKGS) are written in terms of a reference velocity $\mathbf{u}_\alpha = (u_\alpha, v_\alpha)$ at the reference elevation $z = z_\alpha = -0.531h$. In particular the WKGS equations for mass and momentum conservation are written as

$$\eta_t + \nabla \cdot \mathbf{M} = 0, \tag{14}$$

$$\mathbf{u}_{\alpha,t} + (\mathbf{u}_\alpha \cdot \nabla) \mathbf{u}_\alpha + g \nabla \eta + \mathbf{V}_1 + \mathbf{V}_2 = 0, \tag{15}$$

where η is the free surface elevation. \mathbf{M} , \mathbf{V}_1 , and \mathbf{V}_2 are the dispersive Boussinesq terms, given by

$$\begin{aligned}
\mathbf{M} = & (h + \eta) \left[\mathbf{u}_\alpha + \left(\frac{z_\alpha^2}{2} - \frac{1}{6}(h^2 - h\eta + \eta^2) \right) \nabla(\nabla \cdot \mathbf{u}_\alpha) \right] \\
& + (h + \eta) \left[\left(z_\alpha + \frac{1}{2}(h - \eta) \right) \nabla(\nabla \cdot (h\mathbf{u}_\alpha)) \right], \tag{16}
\end{aligned}$$

$$\begin{aligned}
\mathbf{V}_1 = & \frac{1}{2} z_\alpha^2 \nabla(\nabla \cdot \mathbf{u}_\alpha + z_\alpha \nabla(\nabla \cdot (h\mathbf{u}_{\alpha,t}))) \\
& - \nabla \left[\frac{1}{2} \delta^2 \nabla \cdot \mathbf{u}_\alpha + \delta \nabla \cdot (h\mathbf{u}_{\alpha,t}) \right], \tag{17}
\end{aligned}$$

$$\begin{aligned}
\mathbf{V}_2 = & \nabla \left[(z_\alpha - \delta)(\mathbf{u}_\alpha \cdot \nabla)(\nabla \cdot (h\mathbf{u}_\alpha)) + \frac{1}{2}(z_\alpha^2 - \delta^2)(\mathbf{u}_\alpha \cdot \nabla) \right. \\
& \left. \times (\nabla \cdot \mathbf{u}_\alpha) \right] + \frac{1}{2} \nabla [(\nabla \cdot (h\mathbf{u}_\alpha) + \delta \nabla \cdot \mathbf{u}_\alpha)^2], \tag{18}
\end{aligned}$$

where h is the still water depth.

Nwogu's equations are recovered by neglecting nonlinear dispersive terms. The mass conservation equation remains in the form of Eq. (14) but with

$$\begin{aligned}
\mathbf{M} = & (h + \eta) \mathbf{u}_\alpha + \left(\frac{hz_\alpha^2}{2} - \frac{h^3}{6} \right) \nabla(\nabla \cdot \mathbf{u}_\alpha) \\
& + \left(hz_\alpha^2 - \frac{h^2}{2} \right) \nabla(\nabla \cdot (h\mathbf{u}_\alpha)), \tag{19}
\end{aligned}$$

while the equation for momentum conservation becomes

$$\begin{aligned}
\mathbf{u}_{\alpha,t} + (\mathbf{u}_\alpha \cdot \nabla) \mathbf{u}_\alpha + g \nabla \eta + \frac{z_\alpha^2}{2} \nabla(\nabla \cdot \mathbf{u}_{\alpha,t}) \\
+ z_\alpha \nabla(\nabla \cdot (h\mathbf{u}_{\alpha,t})) = 0. \tag{20}
\end{aligned}$$

Linear dispersive properties vary with the choice of z_α . Details on the numerical scheme used in FUNWAVE2D can be found in Wei *et al.*²³

The above equations are only valid for nonbreaking waves and, therefore, need additional approximations of added physics to model the wave breaking. While the mass conservation equation (14) remains unchanged, in Eq. (20) some additional eddy-viscosity terms are added (following Kennedy *et al.*²⁴) so that it becomes

$$\begin{aligned}
\mathbf{u}_{\alpha,t} + (\mathbf{u}_\alpha \cdot \nabla) \mathbf{u}_\alpha + g \nabla \eta + \frac{z_\alpha^2}{2} \nabla(\nabla \cdot \mathbf{u}_{\alpha,t}) \\
+ z_\alpha \nabla(\nabla \cdot (h\mathbf{u}_{\alpha,t})) - \mathbf{R} = 0, \tag{21}
\end{aligned}$$

with $\mathbf{R} = \mathbf{R}_b + \mathbf{R}_s + \mathbf{R}_f$. \mathbf{R}_b represents a dissipative body force due to wave breaking, \mathbf{R}_s accounts for small-scale turbulence dissipation and \mathbf{R}_f accounts for bottom friction. The first two terms have similar dependence on the flow gradients but different intensity determined through eddy viscosities ν_T^b and ν_T^s specific to the two different dissipation mechanisms. Eddy viscosity for the breaking model is given by

$$\nu_T^b = B \delta^2 [(h + \eta) \nabla \cdot \mathbf{M}] \tag{22}$$

with ν_T^b defined through the mixing length coefficient δ and the quantity B , which controls both the occurrence of energy dissipation and the width of the resulting bore front. The

subgrid turbulence eddy viscosity ν_T^s is defined in terms of a mixing coefficient c_m (see Chen *et al.*¹⁰):

$$\nu_T^s = c_m \Delta x \Delta y \left[(U_{,x})^2 + (V_{,y})^2 + \frac{1}{2} (U_{,y} + V_{,x})^2 \right]^{1/2}. \quad (23)$$

In Eq. (23), (U, V) denotes a wave-averaged velocity obtained by averaging \mathbf{u}_α over a suitable period, usually two to three peak wave periods.

If $\hat{\nu}_T = \nu_T^b + \nu_T^s$ is used, the total dissipative force $\mathbf{R}_d = \mathbf{R}_b + \mathbf{R}_s$ is given in component form by

$$R_{dx} = \frac{1}{d} \left([\hat{\nu}_T (u_\alpha d)_{,x}]_{,x} + \frac{1}{2} [\hat{\nu}_T (u_\alpha d)_{,y} + \hat{\nu}_T (v_\alpha d)_{,x}]_{,y} \right), \quad (24)$$

$$R_{dy} = \frac{1}{d} \left([\hat{\nu}_T (v_\alpha d)_{,y}]_{,y} + \frac{1}{2} [\hat{\nu}_T (u_\alpha d)_{,y} + \hat{\nu}_T (v_\alpha d)_{,x}]_{,x} \right) \quad (25)$$

with the total local depth $d = h + \eta = d(x, y, t)$.

Finally, the bottom friction \mathbf{R}_f is written in terms of a friction factor:

$$\mathbf{R}_f = -\frac{f}{d} |\mathbf{u}_\alpha| \mathbf{u}_\alpha. \quad (26)$$

The leading-order vorticity is given by

$$\boldsymbol{\Omega} \equiv \hat{\mathbf{k}} \omega = \hat{\mathbf{k}} (v_{\alpha,x} - u_{\alpha,y}). \quad (27)$$

This quantity depends on the choice of reference elevation z_α and, thus, can differ from depth-averaged vorticity by an

amount proportional to the order of dispersive Boussinesq terms.

The vorticity equation is obtained by taking the curl of the momentum equation (21),

$$\begin{aligned} \nabla \times \mathbf{u}_{\alpha,t} + \nabla \times (\mathbf{u}_\alpha \cdot \nabla) \mathbf{u}_\alpha + \nabla \times \frac{z_\alpha^2}{2} \nabla (\nabla \cdot \mathbf{u}_{\alpha,t}) \\ + \nabla \times z_\alpha \nabla (\nabla \cdot (h \mathbf{u}_{\alpha,t})) = \nabla \times \mathbf{R}, \end{aligned} \quad (28)$$

which becomes

$$\begin{aligned} \frac{D\omega}{Dt} + \omega \nabla \cdot \mathbf{u}_\alpha - z_\alpha \hat{\mathbf{k}} \cdot \{ \nabla \times [(\nabla \cdot \mathbf{u}_{\alpha,t}) \nabla z_\alpha] \} \\ - \hat{\mathbf{k}} \cdot \{ \nabla \times [(\nabla \cdot h \mathbf{u}_{\alpha,t}) \nabla z_\alpha] \} = \hat{\mathbf{k}} \cdot (\nabla \times \mathbf{R}). \end{aligned} \quad (29)$$

The third and fourth terms on the left-hand side of (29) are related to second-order contributions to the specification of vorticity transport, and should not be interpreted as source or sink effects for the leading-order vorticity.

Equations (24) and (25), obtained for the breaking terms, allow for an explicit computation of the last term on the right-hand side of Eq. (29). After some manipulations, reported in Appendix C, we obtain the vorticity equation (C18). Now it is possible to derive the enstrophy transport equation, which reads

$$\begin{aligned} \frac{1}{2} \frac{D\omega^2}{Dt} + \omega^2 \nabla \cdot \mathbf{u}_\alpha = & \underbrace{\omega z_\alpha \hat{\mathbf{k}} \cdot \{ \nabla \times [(\nabla \cdot \mathbf{u}_{\alpha,t}) \nabla z_\alpha] \} + \omega \hat{\mathbf{k}} \cdot \{ \nabla \times [(\nabla \cdot h \mathbf{u}_{\alpha,t}) \nabla z_\alpha] \} + \omega \hat{\mathbf{k}} \cdot \{ \nabla \times (\nabla \hat{\nu}_T \cdot (\nabla \mathbf{u}_\alpha)) \}}_{(D)} \\ & + \underbrace{\omega \hat{\mathbf{k}} \cdot \left\{ \nabla \times \left(\frac{\nabla \hat{\nu}_T}{d} \cdot \mathbf{Y} \right) \right\}}_{(S_F.I)} - \underbrace{\omega \hat{\mathbf{k}} \cdot \left\{ \frac{1}{2} \nabla \times (\nabla \hat{\nu}_T \times \hat{\mathbf{k}} \omega) \right\}}_{(S_F.II)} + \underbrace{\frac{\omega}{d} \hat{\mathbf{k}} \cdot [\nabla \hat{\nu}_T \times \nabla \cdot (d \nabla \mathbf{u}_\alpha)]}_{(S_F.III)} \\ & - \underbrace{\omega \hat{\mathbf{k}} \cdot \left\{ \frac{1}{2} \nabla \times \left(\frac{\nabla \hat{\nu}_T}{d} \times (\nabla d \times \mathbf{u}_\alpha) \right) \right\}}_{(S_F.IV)} + \underbrace{\frac{\omega}{d} \hat{\mathbf{k}} \cdot [\nabla \hat{\nu}_T \times \nabla \cdot (\mathbf{Y})] - \frac{\omega \hat{\nu}_T}{2d^2} \nabla d \cdot [\nabla (\hat{\mathbf{k}} \cdot \nabla d \times \mathbf{u}_\alpha)]}_{(S_F.V)} \\ & + \underbrace{\frac{\omega}{2d} [\nabla \hat{\nu}_T \cdot (\nabla (\hat{\mathbf{k}} \cdot \nabla d \times \mathbf{u}_\alpha))] - \frac{\omega \hat{\nu}_T}{d^2} \hat{\mathbf{k}} \cdot \{ \nabla d \times [d \nabla \cdot (\nabla \mathbf{u}_\alpha) + \nabla \cdot \mathbf{Y}] \}}_{(S_F.IV)} + \underbrace{\frac{\hat{\nu}_T}{2} \nabla \cdot (\omega \nabla \omega)}_{(S_F.V)} \\ & + \underbrace{\frac{1}{2} \frac{\hat{\nu}_T}{d} \omega \nabla^2 (\hat{\mathbf{k}} \cdot \nabla d \times \mathbf{u}_\alpha)}_{(S_F.VI)} - \underbrace{\frac{\hat{\nu}_T}{2} (\nabla \omega)^2}_{(F.I)} + \underbrace{\frac{1}{4} \frac{\hat{\nu}_T}{d} \nabla \omega^2 \cdot \nabla d}_{(F.IIa)} + \underbrace{\frac{1}{2} \frac{\hat{\nu}_T}{d} \omega^2 \nabla^2 d}_{(F.IIb)} - \underbrace{\frac{\hat{\nu}_T}{2} \left(\frac{\omega \nabla d}{d} \right)^2}_{(F.III)} \\ & + \underbrace{\frac{\omega}{2} \nabla \hat{\nu}_T \cdot \nabla \omega}_{(S_F.VI)} + \underbrace{\frac{\omega}{2d} [\nabla \hat{\nu}_T \cdot (\omega \nabla d)]}_{(S_F.VI)} - \underbrace{\frac{\omega \hat{\nu}_T}{d^2} \hat{\mathbf{k}} \cdot [\nabla d \times (\nabla d \cdot \nabla \mathbf{u}_\alpha)]}_{(S_F.VI)} + \underbrace{\omega \hat{\mathbf{k}} \cdot (\nabla \times \mathbf{R}_f)}_{(S_F.VI)}, \end{aligned} \quad (30)$$

where $d=h+\eta$ is the total local depth while \mathbf{Y} is given by Eq. (C14).

The $(S_{F.})$ terms are formally equivalent to the $(S.)$ terms of the wave-averaged model [see Eqs. (8) and (9)]. They are all dependent on the gradient of d because of their strong dependence on the specific modelling of the dissipative force \mathbf{R} .

Terms $(F.)$ are the analogous terms of the T -terms characterized in Eq. (8) for the wave-averaged circulation model and, therefore, they assume an analogous physical meaning. Terms $(F.I)$ and $(F.III)$, which are “negative definite,” are the most important for the enstrophy dissipation process [note that $(F.III)$ and is equal to zero for $\nabla d=0$]. As seen for the wave-averaged model, *a priori* little can be said on the sign of $(F.IIb)$, while term $(F.IIa)$ is again the same production term as in BC04 and in Schär and Smith.²¹

Again, the term D represents the contribution of dispersive terms in the Boussinesq approximation to the representation and transport of vorticity, and should not be interpreted as a direct source or sink mechanism for the enstrophy.

III. GENERATION AND DISSIPATION OF VORTICITY

In this section we analyze the mechanisms of generation/dissipation of vorticity using results obtained by running both the wave-averaged (SHORECIRC) and the wave-resolving (FUNWAVE2D) models. The clearest indicators are quantities which admit positive/negative-definite (respectively, always positive or negative) contributions. These are the enstrophy and the kinetic energy. The evolution of flows over complex bathymetries, like rip channels, as computed by SHORECIRC and FUNWAVE2D, is analyzed in detail and each contribution to the enstrophy equations (8) and (30) is evaluated from the numerical solution.

Numerical simulations have been carried out for three different bathymetries in which bars are placed with different distances to each other, corresponding to the cases used in Kennedy *et al.*⁷ No qualitative differences affecting the present analysis were noted between the cases, and we confine our attention here to the case of the narrowest rip channel.

The numerical wave basin is 15.50 m wide and 18.15 m long. Figure 1 shows the bathymetry. The two rip channels are both 1.80 m wide, while the distance between them is 9.11 m. The submerged bar is placed on a 1:30 sloping beach at 2.95 m off the shore. The still water depths at the crest and at the offshore toe of the bar are 0.057 m and 0.12 m, respectively, while the water depth on the offshore flat bottom is 0.40 m. The bar width in the cross shore direction is 1.10 m while in the long shore direction is 3.45 m for the edge bars and 7.31 m for the central bar.

Regular waves were run with an offshore wave height $H_0=4.5$ cm and a wave period $T=1$ s. The bottom friction is quantified by a friction coefficient $c_f=0.01$. At the lateral boundaries we have imposed wall lateral boundary conditions, while at the seaward boundary of the domain a generating boundary condition has been used. A model grid size of $(\Delta x, \Delta y)=(0.05, 0.05)$ m and time step $\Delta t=0.01$ s have been

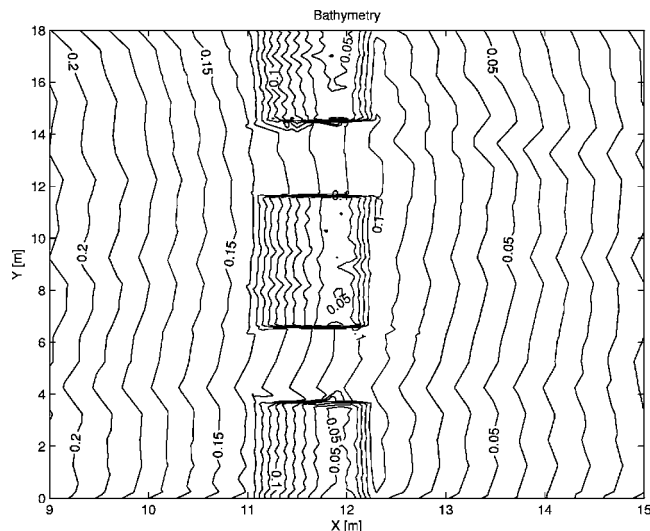


FIG. 1. Topography of the barred beach with two narrow rip channels used for the computations of case (a).

used in all tests. The numerical simulations run with SHORECIRC made use of a depth-uniform velocity configuration to get data comparable with the ones coming from FUNWAVE2D, thus the term CC appearing in Eq. (10) is neglected. All figures refer to the rip current bathymetry (a) and are plotted at the same time $t=60$ s, which is far enough from the initial transient to illustrate typical circulation conditions.

A. The wave-averaged model

We start from the enstrophy equation for the wave-averaged model SHORECIRC, i.e., Eq. (8).

In Fig. 2 (top left panel) the mean water level is plotted together with the velocity field vectors in the case of the rip current, while in the top right panel the vorticity $\bar{\omega}$ field is illustrated. Typical vortical structures can be observed as described by Kennedy *et al.*⁷ The main circulation features are both the bar macrovortices (shed at the breakwater edges and seaward evolving) and the shore macrovortices (located between the shoreline and the breakwater). As expected a weak contribution to the vorticity patterns is given by the shore vortices in the wave-averaged model. The two middle panels give global information, respectively, on the contributions due to the radiation stress forcing and the WC term in the enstrophy equation (8). The radiations stress-related forcing is not positive-definite, therefore it does not provide a source only. However, the enstrophy production is larger on the side of the rip channel both over the bar and shoreward of the bar. Its contribution is also important in proximity of the breaking zone close to the shore. No major differences are observed in the magnitude of the production terms at the edges of the bar and at the lee of them.

This is due to the chosen wave driver, i.e., REF/DIF, based on a parabolic mild slope equation and, thus, represents only orthogonal wave diffraction and influences the production of energy at the lee of the bars. The WC term seems to have more of a dissipative than a productive role and is larger near the corners of the bars and in the middle of

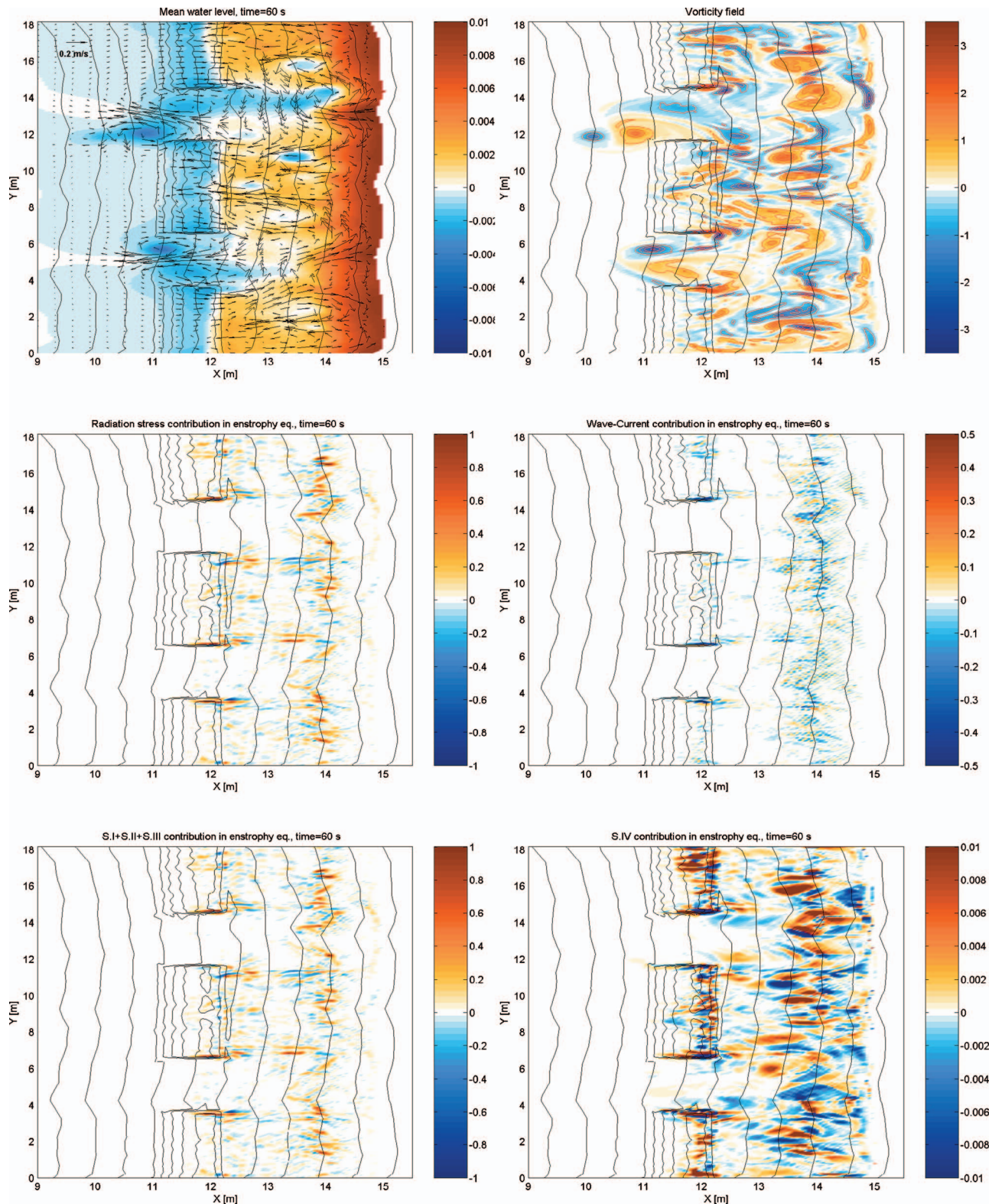


FIG. 2. (Color) Flow structure and main contributions to Eq. (8) ($t=60$ s). From left to right and from top to bottom: mean water level, vorticity field, the S term, the dispersive mixing WC , the $S.I+S.II+S.III$ term and the $S.IV$ term for the enstrophy production.

their shoreward side. Obviously, because of its nature, it is very weak over the bars but is large just shoreward of them. Qualitatively its spatial distribution is very similar to that of the radiation stress forcing. We can observe that in this case WC gives only a small contribution to the enstrophy over the

lateral sides of the bar. This term, also in view of the similar results obtained for all stages of evolution, gives a contribution to the generation/dissipation of vorticity in the rip channel just inshore of the bars.

On the bottom-left panel of Fig. 2 the term $S.I+S.II$

+ $S.III$, representing the portion of the total radiation stress contribution independent of the gradient ∇h of the total water depth, is plotted. We can observe that this portion of the radiation stress forcing is of the same intensity of the total term plotted on the panel above. The last panel of the figure shows the $S.IV$ contribution, proportional to ∇h , to the radiation stress forcing. This is two orders of magnitudes smaller (note the difference in scale) than $S.I+S.II+S.III$ (middle left panel) and it acts both as a source and sink of enstrophy. Consequently $S.I+S.II+S.III$ has a spatial pattern qualitatively similar to the S term with larger positive intensity on the side of the rip channel both over the bars and shoreward of them. The spatial distribution of $S.I+S.II+S.III$ is also qualitatively similar to the WC term, therefore we could conclude that both terms are influenced by the same main forcing. From these results it seems that here the enstrophy generation is dominated by the $1/h$ term rather than the ∇h terms.

This is in opposition to what happens in wave-resolving models in which depth gradients provide the leading force. A complementary description of the contributions to the enstrophy generation is given in Sec. IV in terms of the energy dissipation due to breaking waves. Such description also highlights differences in energy dissipation mechanisms of the two models which provides significant differences in forcing the flow and, in turn, of generating vorticity.

Because of the previous findings, we analyze in more detail the radiation stress contribution due to $S.I$, $S.II$, and $S.III$, separately. $S.I$ and $S.II$ terms are plotted in the upper panels of Fig. 3.

The left upper panel shows the $S.I$ term whose intensity and spatial distribution is similar to that of the total radiation stress forcing. This term seems to give a dissipative contribution only shoreward of the shore-breaking zone ($x \cong 14$ m), dissipation which is locally balanced by the productive role played by the term $S.II$ plotted on the right upper panel of the same figure.

The latter term is really small, close to the bar, and dominates the production of the shore vortices. It represents the contribution in the radiation stress term due to the gradient of the short-wave vorticity $\nabla \omega_w$. Such a term becomes more and more intense in time until it becomes almost stationary. Looking at the evolution in time of the radiation stress forcing, it seems to lose, little by little, intensity before it becomes “quasisteady.”

In the left middle panel of Fig. 3 $S.III$ is plotted. This is smaller than $S.I$ and $S.II$ but it shows the typical distribution of S and $S.I$, therefore we argue that such distribution is mainly due to the $1/h \nabla \cdot \mathbf{u}_w$ term present in both $S.I$ and $S.III$ (here plotted on the right middle panel of Fig. 3), see Eq. (9).

Enstrophy and, thus, vorticity $\tilde{\omega}$ seems to be dissipated mainly by viscous effects. Terms $T.I$ and $T.III$ are, respectively, plotted on the left and right lower panels of Fig. 3, together with the vorticity contours. The dominant dissipative term is $T.I$ while $T.III$, representing the sink effects of the local ∇h , is very small, as well as the production due to a gradient of h . Therefore, for this class of models, it results in the local depth gradient weakly contributing to the main

generation/dissipation mechanisms governing the vorticity dynamics, as described by BC04 for the NSW framework. Note that the dominant dissipation term $T.I$ simply represents the classic dissipation due to eddy viscosity effects, that are similar to the 2D stretching inducing enstrophy cascade, occurring when two equally-signed vortices stretch an oppositely-signed vortex located in between them (see Piatella *et al.*⁵ and Kraichnan¹⁹). The term plotted on the right panel represents the dissipation due to ∇h . This is negative-definite and, like the production term due to ∇h , is very small.

B. The wave-resolving model

In this subsection results from the wave-resolving model FUNWAVE2D are examined focusing on production/dissipation of enstrophy. The bathymetry, grid and time steps are the same as in the SHORECIRC application.

The top row of Fig. 4 shows the instantaneous surface elevation and the corresponding instantaneous vorticity field. To make meaningful comparisons with the results coming from SHORECIRC it is necessary to also analyze the wave-averaged flow. For this purpose a moving average over two short-wave periods has been used. Wave-averaged free surface and vorticity fields are shown in the bottom row of the same figure.

Instantaneous and wave-averaged vorticity are not dramatically different, as also reported in other studies (e.g., Refs. 10 and 14). Although the results are quite similar to the ones coming from SHORECIRC (see Fig. 2), several differences may be pointed out. If two snapshots of the simulation taken at the same time are considered, the travel of the vortex pairs described by the two models seems quite different. In particular SHORECIRC seems to predict a faster migration of the bar vortices.

This behavior, partially influenced by the different treatment of cold-start of the models (wave forcing is ramped up in SHORECIRC but applied instantaneously in FUNWAVE2D), is not of fundamental importance for our analysis, which is mainly focused on evaluating the magnitude of enstrophy generation/dissipation. More importantly, FUNWAVE2D clearly reproduces the main features of a rip current i.e., a feeder, a neck and vortex pairs moving offshore. Such flow organization, especially near the gap tips, is less evident from the results of SHORECIRC (compare with the top-left panel of Fig. 2). The current velocity increases locally on the bars due to the irregularities in the bathymetry. This introduces shear flows and a disruption of the organization of the feeder region especially close to the gap. This effect is still present but less evident close to the shoreline.

In turn, the spatial structure of the vorticity/enstrophy forcing terms is largely influenced by such local effects and FUNWAVE2D predicts two almost symmetric vortices. The characteristics of the vortical structures are largely determined by the structure of the vorticity/enstrophy forcing terms, i.e., by the instantaneous and mean values of R_{bx} and R_{by} which are spatially more coherent than the equivalent forcings of SHORECIRC and, as expected, resemble the structure of the bathymetry itself. These are, respectively,

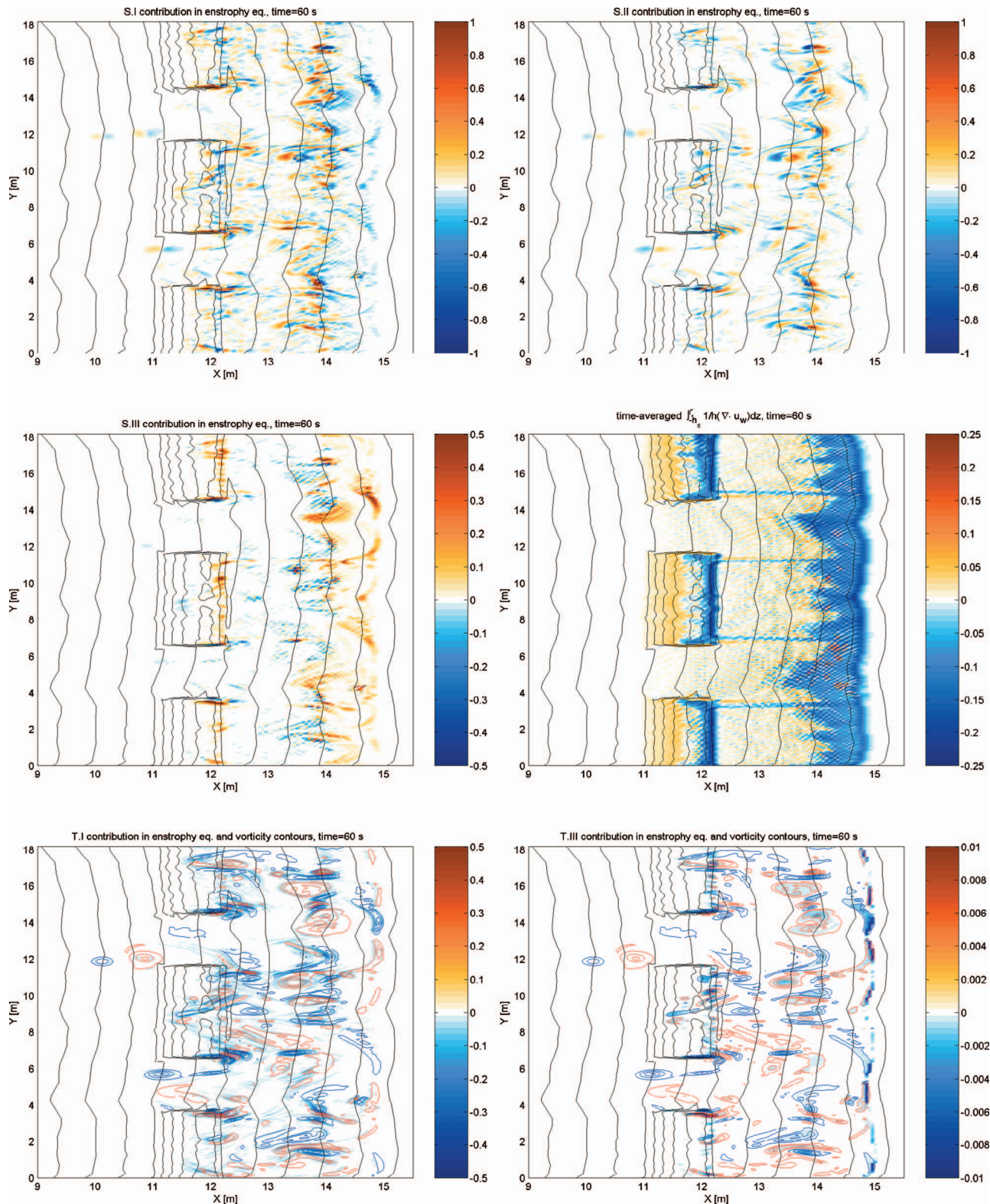


FIG. 3. (Color) Entrophy production. Left upper panel: $S.I$, right upper panel: $S.II$, left middle panel: $S.III$, right middle panel: $\int_{-h_0}^{\xi} \frac{1}{h} \nabla \cdot \mathbf{u}_w dz$. Entrophy dissipation. Left lower panel: $T.I$, right lower panel: $T.III$. Vorticity contours are superposed for ease of inspection.

shown on the top and middle rows of Fig. 5, while the curl of these terms appears in the bottom row of the same figure. This quantity is as an ensemble the source of vorticity as described by the wave-resolving model. The instantaneous values of $\nabla \times \mathbf{R}_b$ and the mean ones are quite different, as

expected, since as the instantaneous values are dependent on the position of the roller at each time step while the wave-averaged ones take into account its path during the time interval used for averaging. Johnson and Pattiaratchi²⁵ have provided further illustration of how the instantaneous struc-

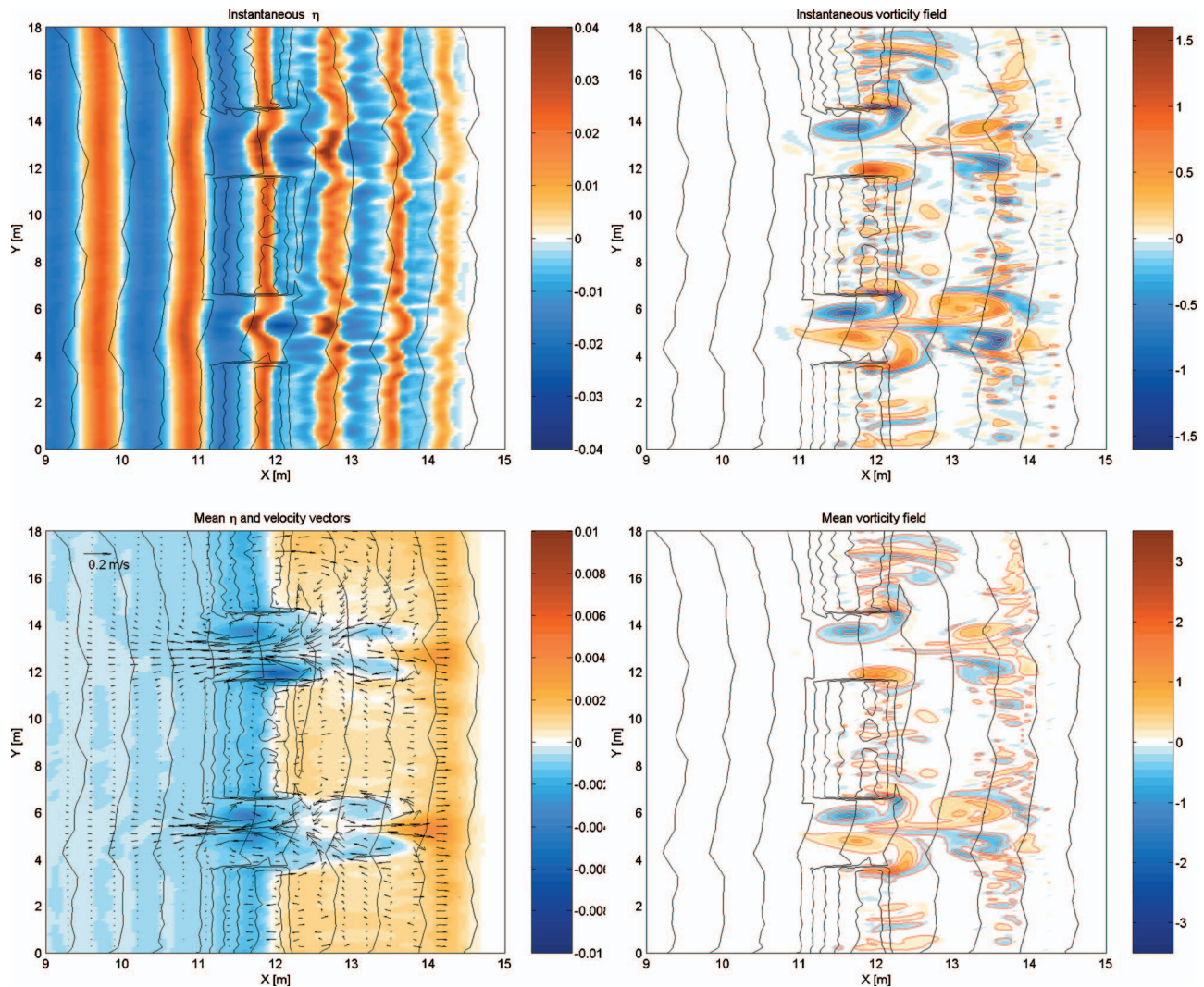


FIG. 4. (Color) Instantaneous (top row) and averaged over two wave periods (bottom row) surface elevation and vorticity fields as computed by FUNWAVE2D ($t=60$ s).

ture of breaking wave crests leads to persistent patches of vorticity in the breaking of random waves on a plane beach. In the present case, the simplicity of the incident wave field guarantees that the wave-breaking generation mechanism should be localized at the rip channel edges and in the regions landward of the channel where wave crest geometry becomes markedly two-dimensional. Note that the vortex cores are not characterized by large values of $\nabla \times \mathbf{R}$.

Vortices generated by differential wave breaking at the bars are a consequence of the spatial structure of the breaking terms. With wave breaking localized on the bars, the dominant vorticity production is represented by the differential breaking itself. In turn the averaged value of the curl of the breaking terms shows how the mean vorticity production and dissipation is localized in space. On the other hand, the production at the edges of the bars predicted by SHORECIRC is rather weak although the vorticity magnitude is higher than that computed by FUNWAVE2D.

Inspection of S_F , which is illustrated in the top panel of Fig. 6 and represents the sum of the contributions to $D\omega^2/Dt$ formally equivalent to the S forcings to $\tilde{\omega}^2$, reveals that such

equivalence is only formal, its size being smaller than S and its spatial structure being very different from that of $\nabla \times \mathbf{R}$. This suggests that, while for the wave-averaged model enstrophy is mainly forced by the considered S terms, the formally equivalent S_F terms represent a minor forcing to ω , with other contributions to $\nabla \times \mathbf{R}$ being more important.

Like the wave-averaged model, the classic viscous dissipation (bottom left panel of Fig. 6) dominates that depend on ∇d (bottom right panel of Fig. 6).

IV. BREAKING WAVE DISSIPATION

To gain further support to the analysis of the previous section the breaking wave dissipation is analyzed as implemented in the two different models following the approaches of Peregrine^{2,3} and Brocchini *et al.*⁶ In particular Peregrine showed, using a bore-like dissipation model, that the rate of energy loss through a single bore is equal to the instantaneous rate of change of circulation around a closed material curve passing once through that bore. In particular the rate of energy loss is

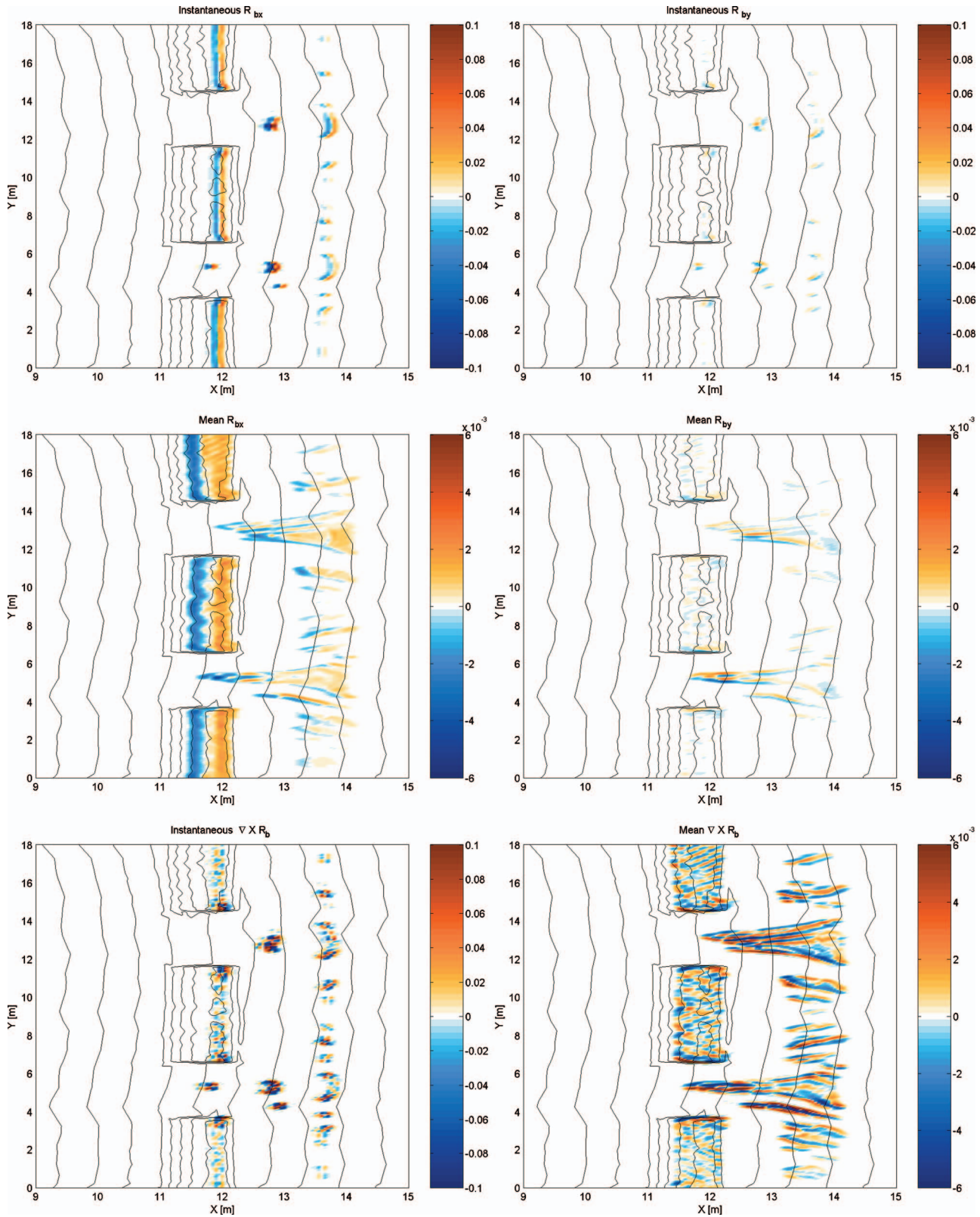


FIG. 5. (Color) Radiation stress forcing as computed by FUNWAVE2D. Top row: instantaneous values of the breaking terms (left panel R_{bx} , right panel R_{by}). Middle row: wave-averaged values of the breaking terms (left panel R_{bx} , right panel R_{by}). Bottom row: the curl of the breaking terms (left panel instantaneous values, right panel wave-averaged ones).

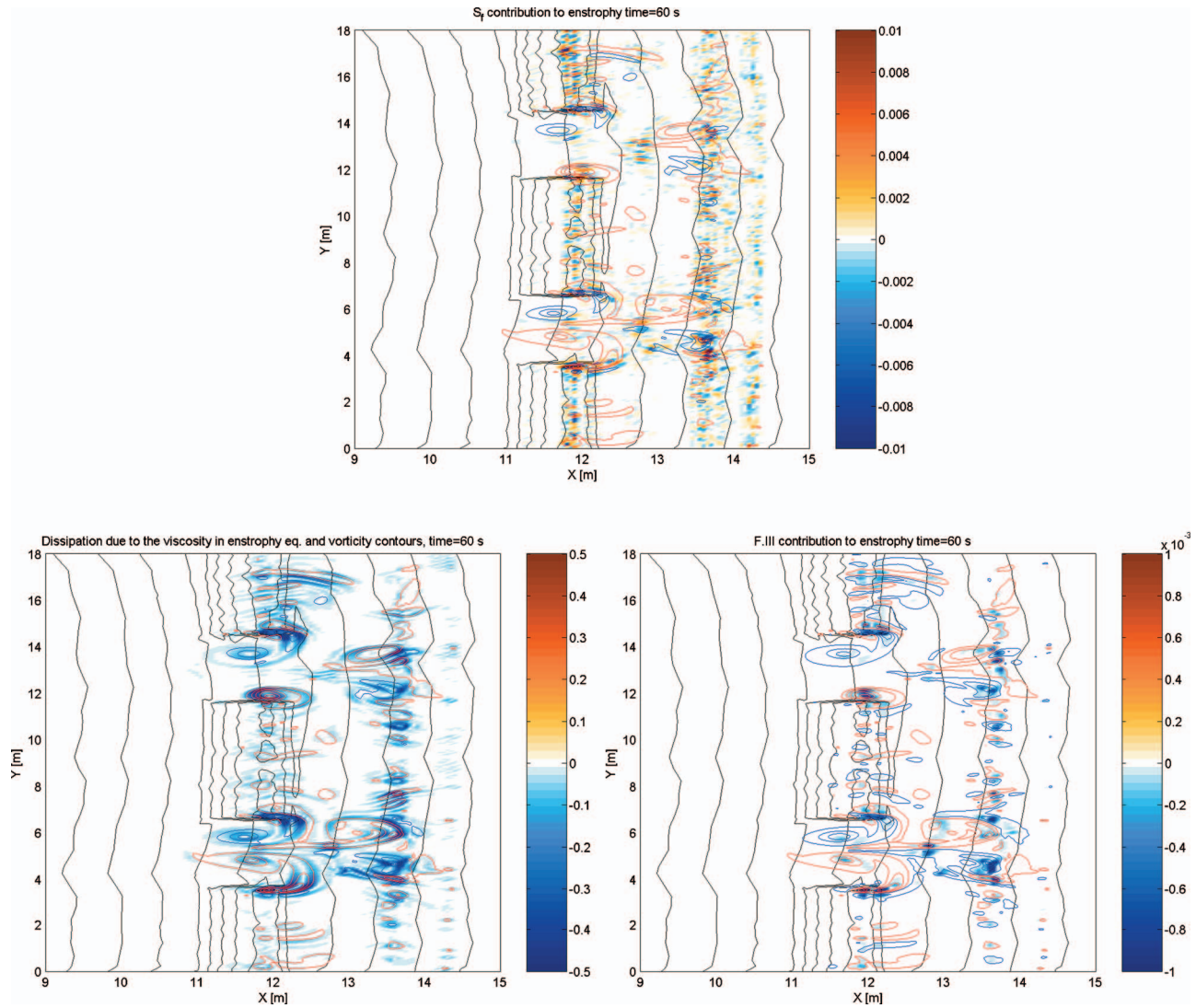


FIG. 6. (Color) Top panel: the S_F term in Eq. (30), proportional to ∇d . Bottom panels: enstrophy dissipation terms $F.I$ (left) and $F.III$ (right).

$$E_D = \frac{D\Gamma}{Dt}, \tag{31}$$

$$\frac{\partial(EC_g)}{\partial x} = -WE, \tag{33}$$

where

$$\Gamma \equiv \oint \tilde{\mathbf{V}} \cdot d\mathbf{l} \quad \text{and} \quad E_D \equiv \oint \mathbf{R} \cdot d\mathbf{l}, \tag{32}$$

$\tilde{\mathbf{V}}=(U, V)$ is the mentioned depth-averaged velocity vector and \mathbf{R} is, in the bore model, the dissipative body force due to turbulent bores.

A. The wave-averaged model

REF/DIF, i.e., the wave driver here forcing SHORE-CIRC, uses the dissipation model proposed by Kirby and Dalrymple.²⁶ For waves propagating shoreward in the x direction the steady form of the energy flux conservation law reads

or, referring to the dissipative body force due to the breaking, \mathbf{R} ,

$$\frac{\partial(EC_g)}{\partial x} = -R_x h C_g, \tag{34}$$

see Brocchini *et al.*⁶ Here (EC_g) is the energy flux, where $E=\rho g H^2/8$ is the average wave energy density per unit of surface area and $C_g=(\sigma/k)(1+2kh/\sinh 2kh)/2$ is the group velocity. k is related to the local depth h by the dispersion relationship $\sigma^2=gk \tanh(kh)$, with $\sigma=2\pi/T$ and T wave period. Assuming the group velocity corresponding to the “stable” energy flux for a broken wave C_{gs} equals C_g , W is written as

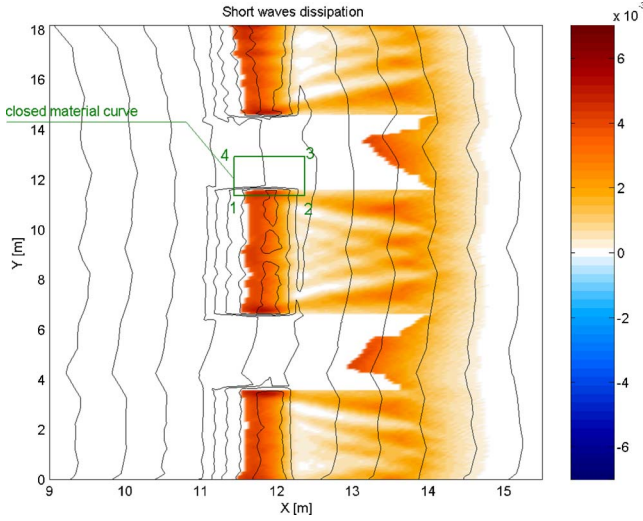


FIG. 7. (Color online) Example of the closed material curve along which E_D is computed in the case of a narrow rip bathymetry.

$$W = \frac{KC_g(1 - (\gamma h/H)^2)}{h} \quad (35)$$

and

$$WE = \frac{\rho g KC_g}{8h} (H^2 - (\gamma h)^2), \quad (36)$$

where H is the local wave height. K and γ are empirical constants, used to measure, respectively, the energy dissipation efficiency and the depth-limited wave height. Dally *et al.*²⁷ estimated the two constant as $K=0.017$ and $\gamma=0.4$.

Following Brocchini *et al.*⁶ in the case of wave-averaged models the rate of energy loss actually computed by the numerical solver is

$$E_D = \oint \mathbf{R} \cdot d\mathbf{l} = \int_1^2 \frac{WE}{hC_g} dx + \int_2^3 \frac{WE}{hC_g} dy + \int_3^4 \frac{WE}{hC_g} dx + \int_4^1 \frac{WE}{hC_g} dy \geq \int_1^2 \frac{WE}{hC_g} dx \quad (37)$$

evaluated along a closed curve as shown in Fig. 7.

Using a bore-type approach, for which 1 and 2 are, respectively, points placed offshore and inshore of the breaking event and being $\hat{h}=(h_1+h_2)/2$, the following estimate of E_D can be given by integrating Eq. (34) in x :

$$E_D \simeq \int_1^2 R_x dx = - \int_1^2 \frac{1}{hC_g} \frac{\partial(EC_g)}{\partial x} dx \simeq \frac{1}{\hat{h}\sqrt{g\hat{h}}} [(EC_g)_1 - (EC_g)_2] \quad (38)$$

where quantities $(EC_g)_1$ and $(EC_g)_2$ are the energy fluxes offshore and inshore of the breaking event, the numerical results coming from the wave driver REF/DIF.

TABLE I. Rate of energy loss computed with Eqs. (37)–(39) in the proximity of the breaking event over the bars in the three different cases: (a) narrow rip topography, (b) wider rip topography, and (c) isolated bar.

Bathymetry	E_D [Eq. (37)] (m ² /s ²)	E_D [Eq. (38)] (m ² /s ²)	E_D [Eq. (39)] (m ² /s ²)
Case (a)	0.0065	0.0223	0.0036
Case (b)	0.0064	0.0229	0.0036
Case (c)	0.0064	0.0228	0.0036

Note that while Eq. (37) gives an upper bound for the dissipation mechanism actually implemented in SHORECIRC, Eq. (38) provides an analytical bore-type representation of the same mechanism.

B. The wave-resolving model

The dominant contributions to the energy flux conservation law for nearly shore-normal waves can be written:

$$\frac{\partial E}{\partial t} + \frac{\partial(EC_g)}{\partial x} = -E_D, \quad (39)$$

where the y direction contributions have been found to be small even near the rip channel. The role of the wave-averaged breaking terms is the same as that of WE in the wave driver [see Eqs. (33) and (34)]. Hence, for the closed circuit of Fig. 7, which does not go round the rip neck, only Eq. (39) gives a contribution to the line integral which is formally identical to Eq. (37). Here the group celerity has been evaluated using the Boussinesq approximation as in Wei and Kirby,²³ while the wave height spatial distribution has been evaluated starting from the free surface envelope obtained over five wave periods.

Table I summarizes the numerical values of the rate of energy loss during the breaking event evaluated both with Eqs. (37)–(39) and with the three different bathymetries, already described in Sec. III, to extend the validity of our results.

The results of Table I have three implications:

- (1) They confirm the findings of Kennedy *et al.*⁷ for which E_D , and consequently Γ , are independent of the global topographic configuration (e.g., isolated structure vs array of structures), the latter only governing the macrovortices motion.
- (2) E_D computed by Eq. (38) gives the upper limit for the energy dissipation and is rather larger than those evaluated by Eqs. (37) and (39). Part of the discrepancy may be due to the choice of the integration path, but this alone is not sufficient to justify the large difference. Such difference might be better explained by the mentioned weakness of the model wave driver for SHORECIRC of “seeing shocks” (see also discussion of Fig. 2 above).
- (3) E_D computed by FUNWAVE2D [Eq. (39)] and by REF/DIF-SHORECIRC [Eq. (37)] is approximately the same,

the wave height estimate being mostly affected by wave-current interaction.

V. CONCLUSIONS

Generation and dissipation of topographically induced wave-breaking forced macrovortices evolving in the coastal zone, have been investigated both analytically and numerically.

Two numerical models for near shore circulation are used: a wave-averaged model, i.e., SHORECIRC, and a wave-resolving model, i.e., FUNWAVE. Because of they predict different vorticity dynamics even if applied at identical wave and topography configurations, an accurate comparison between them is needed to understand the main physical mechanisms governing the 2D vorticity dynamics in the coastal zone and how they are modelled by those two circulation models.

Since no comparison is given here with respect to experimental benchmark flows we are unable to definitely assess which model performs best. However, we highlight the differences in the vorticity/enstrophy production/dissipation mechanisms. This has required an analytical derivation of the vorticity and enstrophy equations for both models. Once the equivalent terms that force and dissipate enstrophy in both models have been identified, they have been quantitatively compared using numerical computations carried out for three typical bathymetries, ranging from an isolated breakwater to a typical rip channel configuration. Results pertaining to the latter configuration have been used both to characterize the flow evolution and compare modalities of enstrophy generation/dissipation.

Quantitative and qualitative differences in the vorticity patterns are evident as reproduced by SHORECIRC and FUNWAVE2D. Wave-resolving computations predict well-structured rip current patterns with feeders, neck, and vortex pairs. The flow structures predicted by SHORECIRC are less symmetric and organized, the rip current feeders being “contaminated” by the overbar flows and the shore vortices interacting with a large number of smaller vortical structures.

The flow spatial structures reflect that of the enstrophy/vorticity forcings, i.e., gradients of the radiation stress in the case of the wave-averaged models and curls of the dissipative body forces in the case of wave-resolving computations. Gradients of radiation stresses, not positive-definite (hence providing also dissipation), are strong over the bar edges and in the whole region between the bars and the shoreline. On the contrary, in excellent agreement with the differential breaking vorticity generation mechanism of Peregrine, the curl of dissipative forces are most intense over the breakwater term.

To analyze in more detail enstrophy generation, equivalent enstrophy-forcing terms characterizing the two models have been analyzed. Due to its nature and to the specific definition of the dissipative body force used in FUNWAVE2D all contributions to the forcing $\nabla \times \mathbf{R}$ contain a gradient of the flow depth which is the basis of the mechanism proven by Peregrine. On the other hand, most of the intensity of the gradient of the radiation stress, which forces

the wave-averaged computations, is provided by contributions depending on the gradient of the wave-induced velocity but virtually independent of depth gradients. Similar differences have also been found when directly inspecting the energy dissipation mechanisms.

It seems clear that while for the wave-resolving models a bore-type energy dissipation forces a differential-breaking vorticity generation mechanism, vorticity in wave-averaged models is essentially produced by currents shearing.

Enstrophy dissipation is much easier to investigate as negative-definite contributions characterize transport equations of enstrophy for both types of models. The results obtained with both the wave-averaged and the wave-resolving models suggest that most of enstrophy dissipation occurs because of the “classical” viscous terms, depth gradients only weakly contributing.

In summary, we hypothesize, on the basis of the above arguments (enstrophy generation/dissipation mechanisms, flow symmetry/asymmetry, energy dissipation mechanism), that the wave-resolving Boussinesq-type might be the better candidate for reproducing near shore flows heavily influenced by large-scale vortical structure. This suggestion is currently being verified on the basis of a quantitative comparison against available experimental data of Eulerian (time series of elevation and velocity) and Lagrangian (statistics of passive tracers) type.

ACKNOWLEDGMENTS

The financial support of the Italian M.I.U.R. through Grant No. INTERLINK-II04C02L8E is acknowledged. J.T.K. was supported by the Office of Naval Research, Coastal Geosciences Program (Contract No. N00014-05-1-0069).

APPENDIX A: DERIVATION OF THE SOURCE AND DISPERSIVE MIXING TERMS FOR WAVE-AVERAGED MODELS

The SHORECIRC model is based on the following depth-integrated, short-wave-averaged governing equation:

$$\frac{\partial \bar{\zeta}}{\partial t} + \frac{\partial Q_i}{\partial x_i} = 0, \quad (\text{A1})$$

$$\begin{aligned} \frac{\partial Q_i}{\partial t} + \frac{\partial}{\partial x_i} \left(\frac{Q_i Q_j}{h} \right) + \frac{1}{\rho} \frac{\partial S_{ij}}{\partial x_i} - \frac{1}{\rho} \frac{\partial T_{ij}}{\partial x_i} + \frac{1}{\rho} \frac{\partial L_{ij}}{\partial x_i} + gh \frac{\partial \bar{\zeta}}{\partial x_j} \\ + \frac{\tau_i^B}{\rho} - \frac{\tau_j^S}{\rho} = 0, \end{aligned} \quad (\text{A2})$$

with indices $i(j)=1,2$. The time- and turbulent-averaged total volume flux is defined by

$$Q_i = \int_{-h_0}^{\bar{\zeta}} V_i dz + \int_{\zeta_t}^{\bar{\zeta}} u_{wt} dz \quad (\text{A3})$$

with ζ_t denote the elevation of the wave through. We assume

$$\overline{\int_{-h_0}^{\zeta_t} u_{wi} dz} = 0, \quad (\text{A4})$$

which implies a definition of wave velocity which produces a net volume flux, described below. Considering the V_i constant above $\bar{\zeta}$, from Eq. (A3) we get

$$Q_i = \int_{-h_0}^{\bar{\zeta}} V_i dz + Q_{wi}, \quad (\text{A5})$$

where Q_{wi} is the volume flux due to the short-wave motion and is defined as

$$Q_{wi} = \overline{\int_{-h_0}^{\bar{\zeta}} u_{wi} dz} = \overline{\int_{\zeta_t}^{\bar{\zeta}} u_{wi} dz}. \quad (\text{A6})$$

The current velocity V_i is divided into a depth-uniform part and a depth-varying part into different ways. Following Van Dongeren and Svendsen²⁸ the total current velocity is split in

$$V_i(x, y, z, t) = \tilde{V}_i(x, y, t) + V_{1i}(x, y, z, t), \quad (\text{A7})$$

where the tilde denotes the depth-uniform part defined as

$$\tilde{V}_i = \frac{1}{h} \int_{-h_0}^{\bar{\zeta}} u_{wi} dz = \frac{Q_i}{h}. \quad (\text{A8})$$

From the definition of Q , Eq. (A5) gives

$$Q_i = \tilde{V}_i h + \int_{-h_0}^{\bar{\zeta}} V_{1i} dz + Q_{wi}, \quad (\text{A9})$$

therefore the second component of Eq. (A7), V_{1i} , accounting for the vertical variation of the currents, satisfies the condition

$$\int_{-h_0}^{\bar{\zeta}} V_{1i} dz = - \int_{\zeta_t}^{\bar{\zeta}} u_{wi} dz = -Q_{wi}. \quad (\text{A10})$$

In (A2) S_{ij} is the total short-wave-induced radiation stress (e.g., Mei²⁹):

$$S_{ij} = \overline{\int_{-h_0}^{\zeta} (p \delta_{ij} + \rho u_{wi} u_{wj}) dz} - \delta_{ij} \frac{1}{2} \rho g h^2, \quad (\text{A11})$$

T_{ij} is the depth-integrated turbulent shear stress, expressed by an eddy viscosity model

$$T_{ij} = \rho h \nu_T \left(\frac{\partial \tilde{V}_j}{\partial x_i} + \frac{\partial \tilde{V}_i}{\partial x_j} \right), \quad (\text{A12})$$

and L_{ij} is the quasi-3D dispersive term, which represents the contribution from the depth-varying currents \mathbf{V}_1 , given by the following expression:

$$L_{ij} = \rho \left[\int_{-h_0}^{\bar{\zeta}} V_{1i} V_{1j} dz + \int_{\zeta_t}^{\bar{\zeta}} (u_{wi} V_{1j} + u_{wj} V_{1i}) dz \right]. \quad (\text{A13})$$

Following Van Dongeren and Svendsen,²⁸ we split the depth-varying part of the velocity into

$$V_{1i} = V_{1i}^{(0)} + V_{1i}^{(1)} \quad \text{with } V_{1i}^{(0)} \gg V_{1i}^{(1)} \quad (\text{A14})$$

and assuming that

$$V_{1i}(z) \approx V_{1i}(\bar{\zeta}) \quad \text{in } \zeta_t \leq z \leq \bar{\zeta}, \quad (\text{A15})$$

we approximate Eq. (A13) as

$$L_{ij} \approx \rho \left[\int_{-h_0}^{\bar{\zeta}} V_{1i} V_{1j} dz + V_{1j}(\bar{\zeta}) Q_{wi} + V_{1i}(\bar{\zeta}) Q_{wj} \right]. \quad (\text{A16})$$

Moreover, through Eq. (A10) we make the following approximation (for more details, see Haas and Svendsen¹²):

$$V_{1i}(\bar{\zeta}) \approx - \frac{Q_{wi}}{h}, \quad (\text{A17})$$

therefore the tensor \mathbf{L} becomes

$$L_{ij} \cong \rho \left[\int_{-h_0}^{\bar{\zeta}} V_{1i} V_{1j} dz - 2 \frac{Q_{wi} Q_{wj}}{h} \right]. \quad (\text{A18})$$

We can now rewrite the mass and momentum conservation equations (A1) and (A2), respectively, in terms of the depth-uniform velocity \tilde{V} , and obtain

$$\frac{\partial \bar{\zeta}}{\partial t} + \frac{\partial}{\partial x_i}(\tilde{V}_i h) = 0, \tag{A19}$$

$$\begin{aligned} \frac{\partial}{\partial t}(\tilde{V}_j h) + \frac{\partial}{\partial x_i}(\tilde{V}_i \tilde{V}_j h) + \frac{1}{\rho} \frac{\partial S_{ij}}{\partial x_i} - \frac{1}{\rho} \frac{\partial T_{ij}}{\partial x_i} + \frac{1}{\rho} \frac{\partial L_{ij}}{\partial x_i} + gh \frac{\partial \bar{\zeta}}{\partial x_j} \\ + \frac{\tau_j^B}{\rho} - \frac{\tau_j^S}{\rho} = 0. \end{aligned} \tag{A20}$$

The vorticity equation for wave-averaged models (e.g., SHORECIRC) is obtained by taking the curl of Eq. (A20), giving (see also Ref. 13):

$$\begin{aligned} \frac{D\tilde{\omega}}{Dt} + \tilde{\omega} \nabla \cdot \tilde{V} = -\frac{1}{\rho} \hat{\mathbf{k}} \cdot \left\{ \nabla \times \left[\frac{1}{h} \nabla \cdot (\mathbf{S} - \mathbf{T} + \mathbf{L}) \right] \right\} \\ + \frac{1}{\rho} \hat{\mathbf{k}} \cdot \left\{ \nabla \times \left[\frac{1}{h} (\boldsymbol{\tau}^S - \boldsymbol{\tau}^B) \right] \right\}. \end{aligned} \tag{A21}$$

1. The source term

In the following we analyze in detail each term starting with the source term represented by the contribution of the radiation stress term:

$$\hat{\mathbf{k}} \cdot \left\{ \nabla \times \left[\frac{1}{h} \nabla \cdot (\mathbf{S}) \right] \right\}. \tag{A22}$$

According to Eq. (A11), the radiation stress can be written as

$$\mathbf{S} = \int_{-h_0}^{\zeta} (\rho \mathbf{I} + \rho \mathbf{G}(\mathbf{u}_w, \mathbf{u}_w)) dz - \frac{1}{2} \rho g h^2 \mathbf{I} \tag{A23}$$

where \mathbf{I} is the identity tensor and $\mathbf{G}(\mathbf{a}, \mathbf{b})$ is the tensor operator defined as

$$\mathbf{G}(\mathbf{a}, \mathbf{b}) \equiv \begin{pmatrix} a_1 b_1 & a_1 b_2 & a_1 b_3 \\ a_2 b_1 & a_2 b_2 & a_2 b_3 \\ a_3 b_1 & a_3 b_2 & a_3 b_3 \end{pmatrix} \tag{A24}$$

for any generic vectors $\mathbf{a}=(a_1, a_2, a_3)$, $\mathbf{b}=(b_1, b_2, b_3)$. Combining Eqs. (A22) and (A23), we get

$$\begin{aligned} \hat{\mathbf{k}} \cdot \left\{ \nabla \times \left[\frac{1}{h} \nabla \cdot \mathbf{S} \right] \right\} \\ = \hat{\mathbf{k}} \cdot \left\{ \nabla \times \left[\frac{1}{h} \nabla \cdot \int_{-h_0}^{\zeta} (\rho \mathbf{G}(\mathbf{u}_w, \mathbf{u}_w)) dz \right] \right\}. \end{aligned} \tag{A25}$$

By using the mentioned composite notation we obtain the following expression for the source term (A22) in which $\mathbf{G}_w = \mathbf{G}(\mathbf{u}_w, \mathbf{u}_w)$:

$$\begin{aligned} \hat{\mathbf{k}} \cdot \left\{ \nabla \times \left[\frac{1}{h} \nabla \cdot \int_{-h_0}^{\zeta} (\rho \mathbf{G}_w) dz \right] \right\} \\ = \rho \hat{\mathbf{k}} \cdot \left[\frac{1}{h} \int_{-h_0}^{\zeta} \nabla \times (\nabla \cdot \mathbf{G}_w) dz \right] + \rho \hat{\mathbf{k}} \cdot \left[\frac{1}{h} \nabla \times \int_{-h_0}^{\zeta} \nabla \cdot \mathbf{G}_w dz \right] + \rho \hat{\mathbf{k}} \cdot \left\{ \nabla \times \left[\frac{1}{h} [\nabla \zeta \cdot \mathbf{G}_w] \right] + \frac{1}{h} [\nabla \zeta \times (\nabla \cdot \mathbf{G}_w)] \right\}_{\zeta} \\ + \rho \hat{\mathbf{k}} \cdot \left\{ \nabla \times \left[\frac{1}{h} [\nabla h_0 \cdot \mathbf{G}_w] \right] + \frac{1}{h} [\nabla h_0 \times (\nabla \cdot \mathbf{G}_w)] \right\}_{-h_0} \\ = \rho \int_{-h_0}^{\zeta} \frac{1}{h} \left(\hat{\mathbf{k}} \cdot [\nabla (\nabla \cdot \mathbf{u}_w) \times \mathbf{u}_w] + \mathbf{u}_w \cdot \nabla \omega_w + 2 \omega_w \nabla \cdot \mathbf{u}_w \right) dz + \rho \hat{\mathbf{k}} \cdot \left[\int_{-h_0}^{\zeta} \nabla \frac{1}{h} \times \nabla \cdot \mathbf{G}_w dz \right] \\ + \rho \hat{\mathbf{k}} \cdot \left\{ \nabla \times \left[\frac{1}{h} [\nabla \zeta \cdot \mathbf{G}_w] \right] + \frac{1}{h} [\nabla \zeta \times (\nabla \cdot \mathbf{G}_w)] \right\}_{\zeta} + \rho \hat{\mathbf{k}} \cdot \left\{ \nabla \times \left[\frac{1}{h} [\nabla h_0 \cdot \mathbf{G}_w] \right] + \frac{1}{h} [\nabla h_0 \times (\nabla \cdot \mathbf{G}_w)] \right\}_{-h_0} \\ = \rho \int_{-h_0}^{\zeta} \frac{1}{h} \left(\hat{\mathbf{k}} \cdot [\nabla (\nabla \cdot \mathbf{u}_w) \times \mathbf{u}_w] + \mathbf{u}_w \cdot \nabla \omega_w + 2 \omega_w \nabla \cdot \mathbf{u}_w \right) dz + \rho \hat{\mathbf{k}} \cdot \int_{-h_0}^{\zeta} \left[(\nabla \cdot \mathbf{u}_w) \left(\nabla \frac{1}{h} \times \mathbf{u}_w \right) + \nabla \frac{1}{h} \times (\mathbf{u}_w \cdot \nabla \mathbf{u}_w) \right] dz \\ + \rho \int_{-h_0}^{\zeta} \omega_w \left(\mathbf{u}_w \cdot \nabla \frac{1}{h} \right) dz + \rho \hat{\mathbf{k}} \cdot \left\{ \nabla \times \left[\frac{1}{h} [\nabla \zeta \cdot \mathbf{G}_w] \right] + \frac{1}{h} [\nabla \zeta \times (\nabla \cdot \mathbf{G}_w)] \right\}_{\zeta} \\ + \rho \hat{\mathbf{k}} \cdot \left\{ \nabla \times \left[\frac{1}{h} [\nabla h_0 \cdot \mathbf{G}_w] \right] + \frac{1}{h} [\nabla h_0 \times (\nabla \cdot \mathbf{G}_w)] \right\}_{-h_0}, \end{aligned} \tag{A26}$$

where ω_w is the vertical component of the short-wave induced vorticity:

$$\mathbf{\Omega}_w \equiv \hat{\mathbf{k}}\omega_w = \hat{\mathbf{k}}(v_{w,x} - u_{w,y}). \quad (\text{A27})$$

2. The dispersive mixing term

Now we analyze the dispersive mixing term used in SHORECIRC as defined by Eq. (A18), where its curl is

$$\begin{aligned} & \hat{\mathbf{k}} \cdot \left\{ \nabla \times \left[\frac{1}{h} \nabla \cdot (\mathbf{L}) \right] \right\} \\ &= \rho \hat{\mathbf{k}} \cdot \left\{ \nabla \times \left[\frac{1}{h} \nabla \cdot \left(\int_{-h_0}^{\bar{\zeta}} \mathbf{G}(\mathbf{V}_1, \mathbf{V}_1) dz \right. \right. \right. \\ & \quad \left. \left. \left. - 2 \frac{\mathbf{G}(\mathbf{Q}_w, \mathbf{Q}_w)}{h} \right) \right] \right\}. \end{aligned} \quad (\text{A28})$$

Here the wave flux \mathbf{Q}_w can be written in terms of a product between a depth-uniform velocity $\hat{\mathbf{V}}$ and the total water depth h :

$$\mathbf{Q}_w = \hat{\mathbf{V}}h, \quad (\text{A29})$$

where the velocity vector $\hat{\mathbf{V}}$ represents the difference between the definition of the depth-uniform velocity in Eq. (A8) and the same as defined by Svendsen *et al.*,⁹ \mathbf{V}_m :

$$\mathbf{V}_m = \frac{\mathbf{Q} - \mathbf{Q}_w}{h}, \quad \text{i.e., } \hat{\mathbf{V}} \equiv \tilde{\mathbf{V}} - \mathbf{V}_m \quad (\text{A30})$$

and $\hat{\omega}$ is its related vorticity $\hat{\mathbf{\Omega}} = \hat{\mathbf{k}}\hat{\omega} = \hat{\mathbf{k}}\hat{v}_x - \hat{u}_y$.

Substitution of definition (A29) in (A28) leads to

$$\begin{aligned} & \hat{\mathbf{k}} \cdot \left\{ \nabla \times \left[\frac{1}{h} \nabla \cdot (\mathbf{L}) \right] \right\} \\ &= \rho \hat{\mathbf{k}} \cdot \left\{ \nabla \times \left[\frac{1}{h} \nabla \cdot \left(\int_{-h_0}^{\bar{\zeta}} \mathbf{G}(\mathbf{V}_1, \mathbf{V}_1) dz \right) \right] \right\} \\ & \quad - 2\rho \hat{\mathbf{k}} \cdot \left\{ \nabla \times \left[\frac{1}{h} \nabla \cdot (h\mathbf{G}(\hat{\mathbf{V}}, \hat{\mathbf{V}})) \right] \right\}. \end{aligned} \quad (\text{A31})$$

Now, defining $\mathbf{G}(\hat{\mathbf{V}}, \hat{\mathbf{V}}) \equiv \hat{\mathbf{G}}$, we analyze only the second term on the RHS of Eq. (A31) which leads to

$$\begin{aligned} & \hat{\mathbf{k}} \cdot \left\{ \nabla \times \left[\frac{1}{h} \nabla \cdot (h\hat{\mathbf{G}}) \right] \right\} = \hat{\mathbf{k}} \cdot \left\{ \nabla \times \left[\frac{\nabla h}{h} \cdot \hat{\mathbf{G}} + \nabla \cdot \hat{\mathbf{G}} \right] \right\} \\ &= \hat{\mathbf{k}} \cdot \left\{ \nabla \times \left[\frac{\nabla h}{h} \cdot \hat{\mathbf{G}} \right] + \nabla \times [\nabla \cdot \hat{\mathbf{G}}] \right\} \\ &= \hat{\mathbf{k}} \cdot \left\{ \hat{\mathbf{V}} \times \left[\nabla \times \left(\hat{\mathbf{V}} \times \frac{\nabla h}{h} \right) \right] - 2\hat{\mathbf{V}} \times \left(\frac{\nabla h}{h} \cdot \nabla \hat{\mathbf{V}} \right) + \hat{\mathbf{V}} \times \left(\frac{(\nabla \cdot \hat{\mathbf{V}}) \nabla h}{h} \right) \right\} \\ & \quad - \hat{\mathbf{k}} \cdot [\hat{\mathbf{V}} \times \nabla(\nabla \cdot \hat{\mathbf{V}})] + \hat{\mathbf{V}} \cdot \nabla \hat{\omega} + 2\hat{\omega} \nabla \cdot \hat{\mathbf{V}}. \end{aligned} \quad (\text{A32})$$

The first term on the RHS of Eq. (A31) can be manipulated as already done in Eq. (A26), therefore, the total dispersive mixing term in the vorticity equation results:

$$\begin{aligned} & \hat{\mathbf{k}} \cdot \left\{ \nabla \times \left[\frac{1}{h} \nabla \cdot (\mathbf{L}) \right] \right\} = \rho \int_{-h_0}^{\bar{\zeta}} \frac{1}{h} (\hat{\mathbf{k}} \cdot [\nabla(\nabla \cdot \mathbf{V}_1) \times \mathbf{V}_1] + \mathbf{V}_1 \cdot \nabla \omega_1 + 2\omega_1 \nabla \cdot \mathbf{V}_1) dz \\ & \quad + \rho \hat{\mathbf{k}} \cdot \int_{-h_0}^{\bar{\zeta}} \left[(\nabla \cdot \mathbf{V}_1) \left(\nabla \frac{1}{h} \times \mathbf{V}_1 \right) + \nabla \frac{1}{h} \times (\mathbf{V}_1 \cdot \nabla \mathbf{V}_1) \right] dz \\ & \quad + \rho \int_{-h_0}^{\bar{\zeta}} \omega_1 \left(\mathbf{V}_1 \cdot \nabla \frac{1}{h} \right) dz + \rho \hat{\mathbf{k}} \cdot \left\{ \nabla \times \left[\frac{1}{h} [\nabla \bar{\zeta} \cdot \mathbf{G}_1] \right] + \frac{1}{h} [\nabla \bar{\zeta} \times (\nabla \cdot \mathbf{G}_1)] \right\}_{\bar{\zeta}} \\ & \quad + \rho \hat{\mathbf{k}} \cdot \left\{ \nabla \times \left[\frac{1}{h} [\nabla h_0 \cdot \mathbf{G}_1] \right] + \frac{1}{h} [\nabla h_0 \times (\nabla \cdot \mathbf{G}_1)] \right\}_{-h_0} \\ & \quad - 2\rho \hat{\mathbf{k}} \cdot \left\{ \hat{\mathbf{V}} \times \left[\nabla \times \left(\hat{\mathbf{V}} \times \frac{\nabla h}{h} \right) \right] - 2\hat{\mathbf{V}} \times \left(\frac{\nabla h}{h} \cdot \nabla \hat{\mathbf{V}} \right) + \hat{\mathbf{V}} \times \left(\frac{(\nabla \cdot \hat{\mathbf{V}}) \nabla h}{h} \right) \right\} \\ & \quad + 2\rho \hat{\mathbf{k}} \cdot [\hat{\mathbf{V}} \times \nabla(\nabla \cdot \hat{\mathbf{V}})] - 2\rho \hat{\mathbf{V}} \cdot \nabla \hat{\omega} - 4\rho \hat{\omega} \nabla \cdot \hat{\mathbf{V}}, \end{aligned} \quad (\text{A33})$$

with $\mathbf{G}_1 = \mathbf{G}(\hat{\mathbf{V}}_1, \hat{\mathbf{V}}_1)$.

3. The turbulent shear stress term

Finally, we analyze the contribution to the vorticity due to the depth-integrated turbulent shear stress tensor \mathbf{T} and that due to the bottom shear stress τ^B . Using the definition of \mathbf{T} given in Eq. (A12) we get

$$\hat{\mathbf{k}} \cdot \left\{ \nabla \times \left[\frac{1}{h} \nabla \cdot (\mathbf{T}) \right] \right\} = \rho \hat{\mathbf{k}} \cdot \left\{ \nabla \times \left[\frac{1}{h} \nabla \cdot (h \nu_T \tilde{\mathbf{T}}) \right] \right\} \quad (\text{A34})$$

which is the same as defined in BC04:

$$\tilde{\mathbf{T}} = \begin{pmatrix} 2\tilde{U}_{,x} & \tilde{U}_{,y} + \tilde{V}_{,x} & 0 \\ \tilde{U}_{,y} + \tilde{V}_{,x} & 2\tilde{V}_{,y} & 0 \\ 0 & 0 & 0 \end{pmatrix} = 2 \nabla \tilde{\mathbf{V}} - \tilde{\mathbf{\Omega}}. \quad (\text{A35})$$

Following their approach we obtain

$$\begin{aligned} \hat{\mathbf{k}} \cdot \left\{ \nabla \times \left[\frac{1}{h} \nabla \cdot (\mathbf{T}) \right] \right\} &= \rho \nu_T \nabla^2 \tilde{\omega} + \rho \nabla \nu_T \cdot \nabla \tilde{\omega} + \rho \frac{\nu_T}{h} \hat{\mathbf{k}} \cdot \left[\left(\nabla - \frac{\nabla h}{h} \right) \times (2 \nabla h \cdot \nabla \tilde{\mathbf{V}} - \nabla h \times \hat{\mathbf{k}} \tilde{\omega}) \right] \\ &+ \rho \frac{\hat{\mathbf{k}}}{h} \cdot [\nabla \nu_T \times (2 \nabla h \cdot \nabla \tilde{\mathbf{V}} - \nabla h \times \hat{\mathbf{k}} \tilde{\omega})] + \rho \hat{\mathbf{k}} \cdot [\nabla \times (2 \nabla \nu_T \cdot \nabla \tilde{\mathbf{V}} - \nabla \nu_T \times \hat{\mathbf{k}} \tilde{\omega})] \\ &+ 2 \rho \hat{\mathbf{k}} \cdot (\nabla \nu_T \times \nabla^2 \tilde{\mathbf{V}}). \end{aligned}$$

4. The bottom friction term

The bottom friction term used in SHORECIRC is given by the linear approximation used by Özkan-Haller and Kirby:³⁰

$$\tau_i^B = \rho \frac{2}{\pi} c_f \frac{|u_0|}{h} \tilde{V}_i, \quad (\text{A36})$$

where c_f is the friction coefficient, which depends on the bottom roughness, and $|u_0|$ is the short-wave particle velocity amplitude evaluated at the bottom. As shown by Zhao *et al.*,¹³ though different formulations of the bottom friction can affect the development of shear waves, the quasi-3D effects on the shear waves due to the vertical variation of the currents remains the same.

Substitution of Eqs. (A26), (A33), and (A36) on the RHS of Eq. (A21) and use of the approximation $\tau^S=0$ leads to the final form of the vorticity equation (A37):

$$\begin{aligned} \frac{D\tilde{\omega}}{Dt} + \tilde{\omega} \nabla \cdot \tilde{\mathbf{V}} &= - \hat{\mathbf{k}} \cdot \overline{\int_{-h_0}^{\zeta} \frac{1}{h} ([\nabla(\nabla \cdot \mathbf{u}_w) \times \mathbf{u}_w]) dz} - \overline{\int_{-h_0}^{\zeta} \frac{1}{h} (\mathbf{u}_w \cdot \nabla \omega_w + 2 \omega_w \nabla \cdot \mathbf{u}_w) dz} \\ &- \hat{\mathbf{k}} \cdot \overline{\int_{-h_0}^{\zeta} \left[(\nabla \cdot \mathbf{u}_w) \left(\nabla \frac{1}{h} \times \mathbf{u}_w \right) + \nabla \frac{1}{h} \times (\mathbf{u}_w \cdot \nabla \mathbf{u}_w) \right] dz} - \overline{\int_{-h_0}^{\zeta} \omega_w \left(\mathbf{u}_w \cdot \nabla \frac{1}{h} \right) dz} \\ &- \hat{\mathbf{k}} \cdot \left\{ \nabla \times \left[\frac{1}{h} [\nabla \zeta \cdot \mathbf{G}_w] \right] + \frac{1}{h} [\nabla \zeta \times (\nabla \cdot \mathbf{G}_w)] \right\}_{\zeta} - \hat{\mathbf{k}} \cdot \left\{ \nabla \times \left[\frac{1}{h} [\nabla h_0 \cdot \mathbf{G}_w] \right] + \frac{1}{h} [\nabla h_0 \times (\nabla \cdot \mathbf{G}_w)] \right\}_{-h_0} \\ &- \overline{\int_{-h_0}^{\zeta} \frac{1}{h} (\hat{\mathbf{k}} \cdot [\nabla(\nabla \cdot \mathbf{V}_1) \times \mathbf{V}_1] + \mathbf{V}_1 \cdot \nabla \omega_1 + 2 \omega_1 \nabla \cdot \mathbf{V}_1) dz} \\ &- \hat{\mathbf{k}} \cdot \overline{\int_{-h_0}^{\zeta} \left[(\nabla \cdot \mathbf{V}_1) \left(\nabla \frac{1}{h} \times \mathbf{V}_1 \right) + \nabla \frac{1}{h} \times (\mathbf{V}_1 \cdot \nabla \mathbf{V}_1) \right] dz} - \overline{\int_{-h_0}^{\zeta} \omega_1 \left(\mathbf{V}_1 \cdot \nabla \frac{1}{h} \right) dz} \end{aligned}$$

$$\begin{aligned}
& -\hat{\mathbf{k}} \cdot \left\{ \nabla \times \left[\frac{1}{h} [\nabla \bar{\zeta} \cdot \mathbf{G}_1] \right] + \frac{1}{h} [\nabla \bar{\zeta} \times (\nabla \cdot \mathbf{G}_1)] \right\}_{\bar{\zeta}} - \hat{\mathbf{k}} \cdot \left\{ \nabla \times \left[\frac{1}{h} [\nabla h_0 \cdot \mathbf{G}_1] \right] \right. \\
& \left. + \frac{1}{h} [\nabla h_0 \times (\nabla \cdot \mathbf{G}_1)] \right\}_{-h_0} + 2\hat{\mathbf{k}} \cdot \left\{ \hat{\mathbf{V}} \times \left[\nabla \times \left(\hat{\mathbf{V}} \times \frac{\nabla h}{h} \right) \right] - 2\hat{\mathbf{V}} \times \left(\frac{\nabla h}{h} \cdot \nabla \hat{\mathbf{V}} \right) + \hat{\mathbf{V}} \times \left(\frac{(\nabla \cdot \hat{\mathbf{V}}) \nabla h}{h} \right) \right\} \\
& - 2\hat{\mathbf{k}} \cdot [\hat{\mathbf{V}} \times \nabla(\nabla \cdot \hat{\mathbf{V}})] + 2\hat{\mathbf{V}} \cdot \nabla \hat{\omega} + 4\hat{\omega} \nabla \cdot \hat{\mathbf{V}} + \nu_T \nabla^2 \hat{\omega} + \nabla \nu_T \cdot \nabla \hat{\omega} + \frac{\nu_T \hat{\mathbf{k}}}{h} \\
& \cdot \left[\left(\nabla - \frac{\nabla h}{h} \right) \times (2 \nabla h \cdot \nabla \tilde{\mathbf{V}} - \nabla h \times \hat{\mathbf{k}} \hat{\omega}) \right] + \frac{1}{h} \hat{\mathbf{k}} \cdot [\nabla \nu_T \times (2 \nabla h \cdot \nabla \tilde{\mathbf{V}} - \nabla h \times \hat{\mathbf{k}} \hat{\omega})] \\
& + \hat{\mathbf{k}} \cdot [\nabla \times (2 \nabla \nu_T \cdot \nabla \tilde{\mathbf{V}} - \nabla \nu_T \times \hat{\mathbf{k}} \hat{\omega})] + 2\hat{\mathbf{k}} \cdot (\nabla \nu_T \times \nabla^2 \tilde{\mathbf{V}}) - \hat{\mathbf{k}} \cdot \left\{ \nabla \times \left[\frac{1}{h} \mathcal{P}^B \right] \right\}. \tag{A37}
\end{aligned}$$

APPENDIX B: POTENTIAL VORTICITY AND POTENTIAL ENSTROPY EQUATION FOR WAVE-AVERAGED MODELS

The vorticity and enstrophy equations can be written in term of the potential vorticity $\tilde{q} = \tilde{\omega}/h$ (hereinafter PV) and the potential enstrophy \tilde{q}^2 , respectively.

The PV equation, after some manipulations described in Appendix A, reads

$$\begin{aligned}
\frac{D\tilde{q}}{Dt} = & -\hat{\mathbf{k}} \cdot \overline{\int_{-h_0}^{\zeta} \frac{1}{h^2} ([\nabla(\nabla \cdot \mathbf{u}_w) \times \mathbf{u}_w]) dz} - \overline{\int_{-h_0}^{\zeta} \frac{1}{h} [\mathbf{u}_w \cdot \nabla q_w + \frac{q_w}{h} (\mathbf{u}_w \cdot \nabla h) + 2q_w \nabla \cdot \mathbf{u}_w] dz} \\
& - \hat{\mathbf{k}} \cdot \overline{\int_{-h_0}^{\zeta} \frac{1}{h} \left[(\nabla \cdot \mathbf{u}_w) \left(\nabla \frac{1}{h} \times \mathbf{u}_w \right) + \nabla \frac{1}{h} \times (\mathbf{u}_w \cdot \nabla \mathbf{u}_w) \right] dz} - \overline{\int_{-h_0}^{\zeta} q_w \left(\mathbf{u}_w \cdot \nabla \frac{1}{h} \right) dz} \\
& - \frac{1}{h} \hat{\mathbf{k}} \cdot \left\{ \nabla \times \left[\frac{1}{h} [\nabla \bar{\zeta} \cdot \mathbf{G}_w] \right] + \frac{1}{h} [\nabla \bar{\zeta} \times (\nabla \cdot \mathbf{G}_w)] \right\}_{\bar{\zeta}} - \frac{1}{h} \hat{\mathbf{k}} \cdot \left\{ \nabla \times \left[\frac{1}{h} [\nabla h_0 \cdot \mathbf{G}_w] \right] + \frac{1}{h} [\nabla h_0 \times (\nabla \cdot \mathbf{G}_w)] \right\}_{-h_0} \\
& - \int_{-h_0}^{\bar{\zeta}} \frac{1}{h} \left(\frac{1}{h} \hat{\mathbf{k}} \cdot [\nabla(\nabla \cdot \mathbf{V}_1) \times \mathbf{V}_1] + \mathbf{V}_1 \cdot \nabla q_1 + \frac{q_1}{h} (\mathbf{V}_1 \cdot \nabla h) + 2q_1 \nabla \cdot \mathbf{V}_1 \right) dz - \hat{\mathbf{k}} \cdot \int_{-h_0}^{\bar{\zeta}} \frac{1}{h} \left[(\nabla \cdot \mathbf{V}_1) \left(\nabla \frac{1}{h} \times \mathbf{V}_1 \right) \right. \\
& \left. + \nabla \frac{1}{h} \times (\mathbf{V}_1 \cdot \nabla \mathbf{V}_1) \right] dz - \int_{-h_0}^{\bar{\zeta}} q_1 \left(\mathbf{V}_1 \cdot \nabla \frac{1}{h} \right) dz - \frac{1}{h} \hat{\mathbf{k}} \cdot \left\{ \nabla \times \left[\frac{1}{h} [\nabla \bar{\zeta} \cdot \mathbf{G}_1] \right] + \frac{1}{h} [\nabla \bar{\zeta} \times (\nabla \cdot \mathbf{G}_1)] \right\}_{\bar{\zeta}} \\
& - \frac{1}{h} \hat{\mathbf{k}} \cdot \left\{ \nabla \times \left[\frac{1}{h} [\nabla h_0 \cdot \mathbf{G}_1] \right] + \frac{1}{h} [\nabla h_0 \times (\nabla \cdot \mathbf{G}_1)] \right\}_{-h_0} + \frac{2}{h} \hat{\mathbf{k}} \cdot \left\{ \hat{\mathbf{V}} \times \left[\nabla \times \left(\hat{\mathbf{V}} \times \frac{\nabla h}{h} \right) \right] - 2\hat{\mathbf{V}} \times \left(\frac{\nabla h}{h} \cdot \nabla \hat{\mathbf{V}} \right) \right. \\
& \left. + \hat{\mathbf{V}} \times \left(\frac{(\nabla \cdot \hat{\mathbf{V}}) \nabla h}{h} \right) \right\} - \frac{2}{h} \hat{\mathbf{k}} \cdot [\hat{\mathbf{V}} \times \nabla(\nabla \cdot \hat{\mathbf{V}})] + 2\hat{\mathbf{V}} \cdot \nabla \hat{q} + 2\frac{\hat{q}}{h} (\hat{\mathbf{V}} \cdot \nabla h) + 4\hat{q} \nabla \cdot \hat{\mathbf{V}} + \frac{\nu_T}{h} (h \nabla^2 \tilde{q} + 2 \nabla h \cdot \nabla \tilde{q} \\
& + \tilde{q} \nabla^2 h) + \nabla \nu_T \cdot \nabla \tilde{q} + \frac{\tilde{q}}{h} \nabla \nu_T \cdot \nabla h + \frac{\nu_T \hat{\mathbf{k}}}{h^2} \cdot \left[\left(\nabla - \frac{\nabla h}{h} \right) \times (2 \nabla h \cdot \nabla \tilde{\mathbf{V}}) \right] - \frac{\nu_T \hat{\mathbf{k}}}{h} \cdot [\nabla \times (\nabla h \times \hat{\mathbf{k}} \tilde{q})] \\
& + \frac{1}{h^2} \hat{\mathbf{k}} \cdot [\nabla \nu_T \times (2 \nabla h \cdot \nabla \tilde{\mathbf{V}})] + \frac{1}{h} \hat{\mathbf{k}} \cdot [\nabla \times (2 \nabla \nu_T \cdot \nabla \tilde{\mathbf{V}})] - \hat{\mathbf{k}} \cdot [\nabla \times (\nabla \nu_T \times \hat{\mathbf{k}} \tilde{q})] + \frac{2}{h} \hat{\mathbf{k}} \cdot (\nabla \nu_T \times \nabla^2 \tilde{\mathbf{V}}) \\
& - \frac{1}{h} \hat{\mathbf{k}} \cdot \left\{ \nabla \times \left[\frac{1}{h} \mathcal{P}^B \right] \right\}, \tag{B1}
\end{aligned}$$

while the enstrophy equation is obtained by a simple multiplication of (B1) by $\tilde{\omega}$.

In the potential enstrophy equation (B2) which follows no (T.III) term, negative-definite and strongly depending on the total depth gradient ∇d , is present. This represents a sink for the enstrophy balance while in the potential enstrophy equation is absorbed into (Tp.I) which describes the potential enstrophy dissipation due to viscous effects, becoming part of the conservative vorticity dynamics,

$$\begin{aligned}
 \frac{1}{2} \frac{D\tilde{q}^2}{Dt} = & -\hat{\mathbf{k}} \cdot \int_{-h_0}^{\zeta} \frac{\tilde{q}}{h^2} \overline{([\mathbf{u}_w \times \nabla(\nabla \cdot \mathbf{u}_w)])} dz - \int_{-h_0}^{\zeta} \frac{\tilde{q}}{h} \overline{\left[\mathbf{u}_w \cdot \nabla q_w + \frac{q_w}{h} (\mathbf{u}_w \cdot \nabla h) + 2q_w \nabla \cdot \mathbf{u}_w \right]} dz \\
 & -\hat{\mathbf{k}} \cdot \int_{-h_0}^{\zeta} \frac{\tilde{q}}{h} \overline{\left[(\nabla \cdot \mathbf{u}_w) \left(\nabla \frac{1}{h} \times \mathbf{u}_w \right) + \nabla \frac{1}{h} \times (\mathbf{u}_w \cdot \nabla \mathbf{u}_w) \right]} dz - \int_{-h_0}^{\zeta} \tilde{q} q_w \overline{\left(\mathbf{u}_w \cdot \nabla \frac{1}{h} \right)} dz \\
 & -\frac{\tilde{q}}{h} \hat{\mathbf{k}} \cdot \left\{ \nabla \times \left[\frac{1}{h} [\nabla \zeta \cdot \mathbf{G}_w] \right] + \frac{1}{h} [\nabla \zeta \times (\nabla \cdot \mathbf{G}_w)] \right\}_{\zeta} - \frac{\tilde{q}}{h} \hat{\mathbf{k}} \cdot \left\{ \nabla \times \left[\frac{1}{h} [\nabla h_0 \cdot \mathbf{G}_w] \right] + \frac{1}{h} [\nabla h_0 \times (\nabla \cdot \mathbf{G}_w)] \right\}_{-h_0} \\
 & - \int_{-h_0}^{\zeta} \frac{\tilde{q}}{h} \left(\frac{1}{h} \hat{\mathbf{k}} \cdot [\mathbf{V}_1 \times \nabla(\nabla \cdot \mathbf{V}_1)] + \mathbf{V}_1 \cdot \nabla q_1 + \frac{q_1}{h} (\mathbf{V}_1 \cdot \nabla h) + 2q_1 \nabla \cdot \mathbf{V}_1 \right) dz \\
 & -\hat{\mathbf{k}} \cdot \int_{-h_0}^{\zeta} \frac{\tilde{q}}{h} \overline{\left[(\nabla \cdot \mathbf{V}_1) \left(\nabla \frac{1}{h} \times \mathbf{V}_1 \right) + \nabla \frac{1}{h} \times (\mathbf{V}_1 \cdot \nabla \mathbf{V}_1) \right]} dz - \int_{-h_0}^{\zeta} \tilde{q} q_1 \overline{\left(\mathbf{V}_1 \cdot \nabla \frac{1}{h} \right)} dz \\
 & -\frac{\tilde{q}}{h} \hat{\mathbf{k}} \cdot \left\{ \nabla \times \left[\frac{1}{h} [\nabla \zeta \cdot \mathbf{G}_1] \right] + \frac{1}{h} [\nabla \zeta \times (\nabla \cdot \mathbf{G}_1)] \right\}_{\zeta} - \frac{\tilde{q}}{h} \hat{\mathbf{k}} \cdot \left\{ \nabla \times \left[\frac{1}{h} [\nabla h_0 \cdot \mathbf{G}_1] \right] + \frac{1}{h} [\nabla h_0 \times (\nabla \cdot \mathbf{G}_1)] \right\}_{-h_0} \\
 & + 2\frac{\tilde{q}}{h} \hat{\mathbf{k}} \cdot \left\{ \hat{\mathbf{v}} \times \left[\nabla \times \left(\hat{\mathbf{v}} \times \frac{\nabla h}{h} \right) \right] - 2\hat{\mathbf{v}} \times \left(\frac{\nabla h}{h} \cdot \nabla \hat{\mathbf{v}} \right) + \hat{\mathbf{v}} \times \left(\frac{(\nabla \cdot \hat{\mathbf{v}}) \nabla h}{h} \right) \right\} - 2\frac{\tilde{q}}{h} \hat{\mathbf{k}} \cdot [\hat{\mathbf{v}} \times \nabla(\nabla \cdot \hat{\mathbf{v}})] \\
 & + 2\tilde{q} \hat{\mathbf{v}} \cdot \nabla \hat{q} + 2\frac{\tilde{q}}{h} \hat{q} (\hat{\mathbf{v}} \cdot \nabla h) + 4h\frac{\tilde{q}}{h} \hat{q} \nabla \cdot \hat{\mathbf{v}} + \nu_T \nabla \cdot (\tilde{q} \nabla \tilde{q}) - \underbrace{\nu_T (\nabla \tilde{q})^2}_{I_{PE}} + \underbrace{\frac{3}{2h} \nu_T \nabla h \cdot \nabla \tilde{q}^2}_{II_{PEa}} + \underbrace{\frac{2}{h} \nu_T \tilde{q}^2 \nabla^2 h}_{II_{PEb}} \\
 & + \tilde{q} \nabla \nu_T \cdot \nabla \tilde{q} + \frac{\tilde{q}^2}{h} \nabla \nu_T \cdot \nabla h + \frac{\nu_T \tilde{q}}{h^2} \hat{\mathbf{k}} \cdot \left[\left(\nabla - \frac{\nabla h}{h} \right) \times (2 \nabla h \cdot \nabla \tilde{\mathbf{V}}) \right] + \frac{\tilde{q}}{h^2} \hat{\mathbf{k}} \cdot [\nabla \nu_T \times (2 \nabla h \cdot \nabla \tilde{\mathbf{V}})] \\
 & + \frac{\tilde{q}}{h} \hat{\mathbf{k}} \cdot [\nabla \times (2 \nabla \nu_T \cdot \nabla \tilde{\mathbf{V}})] - \tilde{q} \hat{\mathbf{k}} \cdot [\nabla \times (\nabla \nu_T \times \hat{\mathbf{k}} \tilde{q})] + 2\frac{\tilde{q}}{h} \hat{\mathbf{k}} \cdot (\nabla \nu_T \times \nabla^2 \tilde{\mathbf{V}}) - \frac{\tilde{q}}{h} \hat{\mathbf{k}} \cdot \left[\nabla \times \left[\frac{1}{h} \boldsymbol{\tau}^B \right] \right]. \tag{B2}
 \end{aligned}$$

(Tp.I), (Tp.IIa), and (Tp.IIb) are analogous terms of (T.I), (T.IIa), and (T.IIb) in (8) and (12).

APPENDIX C: DERIVATION OF THE VORTICITY EQUATION FOR WAVE-RESOLVING MODELS

Expressions (24) and (25) allow for an explicit computation of the last terms on the right-hand side of (29):

$$\hat{\mathbf{k}} \cdot (\nabla \times \mathbf{R}) = \hat{\mathbf{k}} \cdot \left\{ \nabla \times \left[\frac{1}{d} \nabla \cdot \left(\frac{1}{2} \hat{\nu}_T \hat{\tilde{T}} \right) \right] \right\}; \tag{C1}$$

in which the tensor $\hat{\tilde{T}}$ is

$$\begin{aligned}
 \hat{\tilde{T}} & \equiv \begin{pmatrix} 2(du_\alpha)_x & ((du_\alpha)_y + (dv_\alpha)_x) & 0 \\ ((du_\alpha)_y + (dv_\alpha)_x) & 2(dv_\alpha)_y & 0 \\ 0 & 0 & 0 \end{pmatrix} \\
 & = \tilde{\tilde{T}} + d\tilde{T} = 2 \nabla (\mathbf{u}_\alpha d) - \mathbf{\Omega}_d, \tag{C2}
 \end{aligned}$$

where $\tilde{\tilde{T}}$ is the same as defined by BC04:

$$\tilde{\tilde{T}} \equiv \begin{pmatrix} 2u_{\alpha x} & u_{\alpha y} + v_{\alpha x} & 0 \\ u_{\alpha y} + v_{\alpha x} & 2v_{\alpha y} & 0 \\ 0 & 0 & 0 \end{pmatrix} = 2 \nabla \mathbf{u}_\alpha - \mathbf{\Omega}; \tag{C3}$$

and

$$\mathbf{\Omega}_d \equiv \begin{pmatrix} 0 & -\omega_d & 0 \\ \omega_d & 0 & 0 \\ 0 & 0 & 0 \end{pmatrix},$$

$$\omega_d = (dv)_{,x} - (du)_{,y} = d\omega + v_\alpha d_{,x} - u_\alpha d_{,y}; \tag{C4}$$

$$\tilde{\tilde{T}} = \begin{pmatrix} 2u(d)_{,x} & (u_\alpha(d)_{,y} + v_\alpha(d)_{,x}) & 0 \\ (u_\alpha(d)_{,y} + v_\alpha(d)_{,x}) & 2v_\alpha(d)_{,y} & 0 \\ 0 & 0 & 0 \end{pmatrix}. \tag{C5}$$

Therefore \mathbf{R} becomes

$$\mathbf{R} = \frac{1}{2d} \nabla \cdot (\hat{\nu}_T \hat{\tilde{T}}) = \frac{1}{2d} \nabla \cdot (\hat{\nu}_T \tilde{\tilde{T}}) + \mathbf{F}, \tag{C6}$$

where \mathbf{F} is the vector of dissipative body forces related with the depth-averaged, effective stress tensor \mathbf{T} , as defined in BC04: $\mathbf{T} = \hat{v}_T \hat{\mathbf{T}}$, and $\hat{\mathbf{T}} = 2(\nabla(d\mathbf{u}_\alpha) - d\nabla\mathbf{u}_\alpha) - (\mathbf{\Omega}_d - d\mathbf{\Omega})$.

Using Eq. (C6) with $\mathbf{R}_1 = \frac{1}{2d} \nabla \cdot (\hat{v}_T \hat{\mathbf{T}})$ the following holds:

$$\hat{\mathbf{k}} \cdot (\nabla \times \mathbf{R}) = \hat{\mathbf{k}} \cdot (\nabla \times \mathbf{R}_1) + \hat{\mathbf{k}} \cdot (\nabla \times \mathbf{F}), \quad (\text{C7})$$

where the results of $\hat{\mathbf{k}} \cdot (\nabla \times \mathbf{F})$ lead to the results already obtained by BC04. In the following we analyze the total dissipation term:

$$\begin{aligned} \hat{\mathbf{k}} \cdot (\nabla \times \mathbf{R}_1) &= \hat{\mathbf{k}} \cdot \left\{ \nabla \times \left[\frac{1}{2d} \nabla \cdot (\hat{v}_T \hat{\mathbf{T}}) \right] \right\} \\ &= \hat{\mathbf{k}} \cdot \frac{1}{2} \left\{ \nabla \times \left[\frac{\nabla \hat{v}_T}{d} \cdot \hat{\mathbf{T}} + \frac{\hat{v}_T}{d} \nabla \cdot \hat{\mathbf{T}} \right] \right\} = \hat{\mathbf{k}} \cdot \left\{ \nabla \times \left[\frac{\nabla \hat{v}_T}{d} \cdot \left(\nabla(d\mathbf{u}_\alpha) - \frac{1}{2} \mathbf{\Omega}_d \right) \right] \right\} + \hat{\mathbf{k}} \cdot \frac{1}{2} \left\{ \nabla \times \left[\frac{\hat{v}_T}{d} \nabla \cdot \hat{\mathbf{T}} \right] \right\} \\ &= \hat{\mathbf{k}} \cdot \left\{ \nabla \times \left[\frac{\nabla \hat{v}_T}{d} \cdot \nabla(d\mathbf{u}_\alpha) \right] - \nabla \times \left[\frac{\nabla \hat{v}_T}{d} \cdot \frac{1}{2} \mathbf{\Omega}_d \right] \right\} + \hat{\mathbf{k}} \cdot \frac{1}{2} \left\{ \nabla \frac{\hat{v}_T}{d} \times [\nabla \cdot \hat{\mathbf{T}}] + \frac{\hat{v}_T}{d} \nabla \times [\nabla \cdot \hat{\mathbf{T}}] \right\} \end{aligned} \quad (\text{C8})$$

for any 2D vector \mathbf{f} we can use the following results:

$$\mathbf{f} \cdot \mathbf{\Omega}_d = \mathbf{f} \times (\hat{\mathbf{k}} \omega_d), \quad (\text{C9})$$

$$\hat{\mathbf{k}} \cdot \{ \nabla \times [\nabla \cdot \hat{\mathbf{T}}] \} = \nabla^2 \omega_d, \quad (\text{C10})$$

$$\nabla \hat{v}_T \times (\nabla \cdot \mathbf{\Omega}_d) = -\hat{\mathbf{k}} \nabla \hat{v}_T \cdot \nabla \omega_d. \quad (\text{C11})$$

which substituted above lead to

$$\begin{aligned} \hat{\mathbf{k}} \cdot (\nabla \times \mathbf{R}) &= \hat{\mathbf{k}} \cdot \left\{ \nabla \times \left[\frac{\nabla \hat{v}_T}{d} \cdot \nabla(d\mathbf{u}_\alpha) - \frac{1}{2} \frac{\nabla \hat{v}_T}{d} \times (\hat{\mathbf{k}} \omega_d) \right] \right\} + \hat{\mathbf{k}} \cdot \frac{1}{2} \left\{ \left[\frac{\nabla \hat{v}_T}{d} - \frac{\hat{v}_T \nabla d}{d^2} \right] \times [\nabla \cdot \hat{\mathbf{T}}] \right\} + \frac{1}{2} \frac{\hat{v}_T}{d} \nabla^2 \omega_d \\ &= \hat{\mathbf{k}} \cdot \left\{ \nabla \times \left[\frac{\nabla \hat{v}_T}{d} \cdot \nabla(d\mathbf{u}_\alpha) - \frac{1}{2} \frac{\nabla \hat{v}_T}{d} \times (\hat{\mathbf{k}} \omega_d) \right] \right\} + \frac{1}{d} \hat{\mathbf{k}} \cdot [\nabla \hat{v}_T \times \nabla \cdot \nabla(d\mathbf{u}_\alpha)] + \frac{1}{2d} \nabla \hat{v}_T \cdot \nabla \omega_d \\ &\quad + \frac{1}{2} \frac{\hat{v}_T}{d} \nabla^2 \omega_d - \frac{\hat{v}_T}{d^2} \hat{\mathbf{k}} \cdot [\nabla d \times \nabla \cdot \nabla(d\mathbf{u}_\alpha)] - \frac{\hat{v}_T}{2d^2} \nabla d \cdot \nabla \omega_d. \end{aligned} \quad (\text{C12})$$

Considering Eq. (C4) and the following terms:

$$\nabla(d\mathbf{u}_\alpha) = d \nabla \mathbf{u}_\alpha + \mathbf{Y}, \quad (\text{C13})$$

with

$$\mathbf{Y} = \begin{pmatrix} u_\alpha(d)_{,x} & u_\alpha(d)_{,y} & 0 \\ v_\alpha(d)_{,x} & v_\alpha(d)_{,y} & 0 \\ 0 & 0 & 0 \end{pmatrix}, \quad (\text{C14})$$

$$\nabla(d\omega) = d \nabla \omega + \omega \nabla d, \quad (\text{C15})$$

$$\nabla^2(d\omega) = d \nabla^2 \omega + 2 \nabla \omega \nabla d + \omega \nabla^2 d, \quad (\text{C16})$$

lead us to rewrite Eq. (C12) as

$$\begin{aligned} \hat{\mathbf{k}} \cdot (\nabla \times \mathbf{R}) &= \hat{\mathbf{k}} \cdot \{ \nabla \times (\nabla \hat{v}_T \cdot (\nabla \mathbf{u}_\alpha)) \} + \hat{\mathbf{k}} \cdot \left\{ \nabla \times \left(\frac{\nabla \hat{v}_T}{d} \cdot \mathbf{Y} \right) \right\} - \frac{\hat{v}_T}{2d} \nabla d \cdot \nabla \omega + \frac{1}{2} \hat{v}_T \nabla^2 \omega \\ &\quad - \hat{\mathbf{k}} \cdot \left\{ \frac{1}{2} \nabla \times \left[\nabla \hat{v}_T \times \hat{\mathbf{k}} \omega + \frac{\nabla \hat{v}_T}{d} \times (\nabla d \times \mathbf{u}_\alpha) \right] \right\} + \frac{1}{d} \hat{\mathbf{k}} \cdot [\nabla \hat{v}_T \times \nabla \cdot (d \nabla \mathbf{u}_\alpha + \mathbf{Y})] + \frac{1}{2} \nabla \hat{v}_T \cdot \nabla \omega \\ &\quad + \frac{1}{2d} [\nabla \hat{v}_T \cdot (\omega \nabla d + \nabla(\hat{\mathbf{k}} \cdot \nabla d \times \mathbf{u}_\alpha))] - \frac{\hat{v}_T}{d^2} \hat{\mathbf{k}} \cdot [\nabla d \times \nabla \cdot (d \nabla \mathbf{u}_\alpha + \mathbf{Y})] - \frac{\hat{v}_T}{2d^2} [\nabla d \cdot (\omega \nabla d + \nabla(\hat{\mathbf{k}} \cdot \nabla d \times \mathbf{u}_\alpha))] \end{aligned}$$

$$+ \frac{1}{2} \frac{\hat{v}_T}{d} [2 \nabla \omega \cdot \nabla d + \omega \nabla^2 d + \nabla^2 (\hat{\mathbf{k}} \cdot \nabla d \times \mathbf{u}_\alpha)]. \quad (\text{C17})$$

Substitution of Eq. (C17) on the right-hand side of Eq. (29) leads to the vorticity equation:

$$\begin{aligned} \frac{D\omega}{Dt} + \omega \nabla \cdot \mathbf{u}_\alpha = & + z_\alpha \hat{\mathbf{k}} \cdot \{ \nabla \times [(\nabla \cdot \mathbf{u}_{\alpha,t}) \nabla z_\alpha] \} + \hat{\mathbf{k}} \cdot \{ \nabla \times [(\nabla \cdot h\mathbf{u}_{\alpha,t}) \nabla z_\alpha] \} + \hat{\mathbf{k}} \cdot \{ \nabla \times (\nabla \hat{v}_T \cdot (\nabla \mathbf{u}_\alpha)) \} \\ & + \hat{\mathbf{k}} \cdot \left\{ \nabla \times \left(\frac{\nabla \hat{v}_T}{d} \cdot \mathbf{Y} \right) \right\} - \frac{\hat{v}_T}{2d} \nabla d \cdot \nabla \omega + \frac{1}{2} \hat{v}_T \nabla^2 \omega - \hat{\mathbf{k}} \cdot \left\{ \frac{1}{2} \nabla \times \left[\nabla \hat{v}_T \times \hat{\mathbf{k}} \omega + \frac{\nabla \hat{v}_T}{d} \times (\nabla d \times \mathbf{u}_\alpha) \right] \right\} \\ & + \frac{1}{d} \hat{\mathbf{k}} \cdot [\nabla \hat{v}_T \times \nabla \cdot (d \nabla \mathbf{u}_\alpha + \mathbf{Y})] + \frac{1}{2} \nabla \hat{v}_T \cdot \nabla \omega + \frac{1}{2d} [\nabla \hat{v}_T \cdot (\omega \nabla d + \nabla (\hat{\mathbf{k}} \cdot \nabla d \times \mathbf{u}_\alpha))] \\ & - \frac{\hat{v}_T}{d^2} \hat{\mathbf{k}} \cdot [\nabla d \times \nabla \cdot (d \nabla \mathbf{u}_\alpha + \mathbf{Y})] - \frac{\hat{v}_T}{2d^2} [\nabla d \cdot (\omega \nabla d + \nabla (\hat{\mathbf{k}} \cdot \nabla d \times \mathbf{u}_\alpha))] \\ & + \frac{1}{2} \frac{\hat{v}_T}{d} [2 \nabla \omega \cdot \nabla d + \omega \nabla^2 d + \nabla^2 (\hat{\mathbf{k}} \cdot \nabla d \times \mathbf{u}_\alpha)]. \end{aligned} \quad (\text{C18})$$

APPENDIX D: POTENTIAL VORTICITY AND POTENTIAL ENSTROPY EQUATION FOR WAVE-RESOLVING MODELS

Once again, as it occurs for the wave-averaged model (e.g., SHORECIRC), the (F.III) term is absorbed into the dissipation term (Fp.I) for the equation employing the PV instead of ω , in complete analogy with the respective (T.III) and (Tp.I) terms. The potential vorticity is still a function of z_α and here is defined as $q = \omega/d$, and the PV equation reads

$$\begin{aligned} \frac{Dq}{Dt} + \frac{q}{d^2} (\eta_t + \nabla \cdot (d\mathbf{u}_\alpha)) = & + \frac{z_\alpha \hat{\mathbf{k}}}{d} \cdot \{ \nabla \times [(\nabla \cdot \mathbf{u}_{\alpha,t}) \nabla z_\alpha] \} + \frac{1}{d} \hat{\mathbf{k}} \cdot \{ \nabla \times [(\nabla \cdot h\mathbf{u}_{\alpha,t}) \nabla z_\alpha] \} + \frac{1}{d} \hat{\mathbf{k}} \cdot \{ \nabla \times (\nabla \hat{v}_T \cdot (\nabla \mathbf{u}_\alpha)) \} \\ & + \frac{1}{d} \hat{\mathbf{k}} \cdot \left\{ \nabla \times \left(\frac{\nabla \hat{v}_T}{d} \cdot \mathbf{Y} \right) \right\} - \hat{\mathbf{k}} \cdot \left\{ \frac{1}{2} \nabla \times [\nabla \hat{v}_T \times \hat{\mathbf{k}} q] \right\} - \frac{1}{d} \hat{\mathbf{k}} \cdot \left\{ \frac{1}{2} \nabla \times \left[\frac{\nabla \hat{v}_T}{d} \times (\nabla d \times \mathbf{u}_\alpha) \right] \right\} \\ & + \frac{1}{d^2} \hat{\mathbf{k}} \cdot [\nabla \hat{v}_T \times \nabla \cdot (d \nabla \mathbf{u}_\alpha + \mathbf{Y})] + \frac{1}{2} \nabla \hat{v}_T \cdot \nabla q + \frac{1}{2} \frac{\hat{v}_T}{d^2} [\nabla^2 (\hat{\mathbf{k}} \cdot \nabla d \times \mathbf{u}_\alpha)] \\ & + \frac{1}{2d} \left[\nabla \hat{v}_T \cdot \left(3q \nabla d + \frac{1}{d} \nabla (\hat{\mathbf{k}} \cdot \nabla d \times \mathbf{u}_\alpha) \right) \right] - \frac{\hat{v}_T}{d^3} \hat{\mathbf{k}} \cdot [\nabla d \times \nabla \cdot (d \nabla \mathbf{u}_\alpha + \mathbf{Y})] \\ & + \frac{\hat{v}_T}{2d} [2q \nabla^2 d + 3 \nabla d \cdot \nabla q + d \nabla^2 q] - \frac{\hat{v}_T}{2d^3} [\nabla d \cdot \nabla (\hat{\mathbf{k}} \cdot \nabla d \times \mathbf{u}_\alpha)]. \end{aligned} \quad (\text{D1})$$

The potential enstrophy equation simply follows from Eq. (D1) and reads

$$\begin{aligned} \frac{1}{2} \frac{Dq^2}{Dt} + \frac{q^2}{d^2} (\eta_t + \nabla \cdot (d\mathbf{u}_\alpha)) = & + \frac{q}{d} z_\alpha \hat{\mathbf{k}} \cdot \{ \nabla \times [(\nabla \cdot \mathbf{u}_{\alpha,t}) \nabla z_\alpha] \} + \frac{q}{d} \hat{\mathbf{k}} \cdot \{ \nabla \times [(\nabla \cdot h\mathbf{u}_{\alpha,t}) \nabla z_\alpha] \} + \frac{\hat{v}_T}{2} \nabla \cdot (q \nabla q) \\ & + \frac{q}{d} \hat{\mathbf{k}} \cdot \{ \nabla \times (\nabla \hat{v}_T \cdot (\nabla \mathbf{u}_\alpha)) \} + \frac{q}{d} \hat{\mathbf{k}} \cdot \left\{ \nabla \times \left(\frac{\nabla \hat{v}_T}{d} \cdot \mathbf{Y} \right) \right\} + \frac{q}{2} \nabla \hat{v}_T \cdot \nabla q \\ & - q \hat{\mathbf{k}} \cdot \left\{ \frac{1}{2} \nabla \times [\nabla \hat{v}_T \times \hat{\mathbf{k}} q] \right\} - \frac{q}{d} \hat{\mathbf{k}} \cdot \left\{ \frac{1}{2} \nabla \times \left[\frac{\nabla \hat{v}_T}{d} \times (\nabla d \times \mathbf{u}_\alpha) \right] \right\} \\ & + \frac{q}{d^2} \hat{\mathbf{k}} \cdot [\nabla \hat{v}_T \times \nabla \cdot (d \nabla \mathbf{u}_\alpha + \mathbf{Y})] - \frac{\hat{v}_T q}{d^3} \hat{\mathbf{k}} \cdot [\nabla d \times \nabla \cdot (d \nabla \mathbf{u}_\alpha + \mathbf{Y})] \\ & + \frac{q}{2d} \left[\nabla \hat{v}_T \cdot \left(3q \nabla d + \frac{1}{d} \nabla (\hat{\mathbf{k}} \cdot \nabla d \times \mathbf{u}_\alpha) \right) \right] - \underbrace{\frac{\hat{v}_T}{2} (\nabla q)^2}_{I_{PE}} + \underbrace{\frac{3\hat{v}_T}{4d} \nabla d \cdot \nabla q^2}_{II_{PEa}} + \underbrace{\hat{v}_T \frac{q^2}{d} \nabla^2 d}_{III_{PEb}} \\ & - \frac{\hat{v}_T q}{2 d^3} [\nabla d \cdot \nabla (\hat{\mathbf{k}} \cdot \nabla d \times \mathbf{u}_\alpha)] + \frac{\hat{v}_T q}{2 d^2} [\nabla^2 (\hat{\mathbf{k}} \cdot \nabla d \times \mathbf{u}_\alpha)]. \end{aligned} \quad (\text{D2})$$

- ¹M. Brocchini and M. Colombini, "A note on the decay of vorticity in shallow flow calculations," *Phys. Fluids* **16**, 2469 (2004).
- ²D. H. Peregrine, "Surf zone currents," *Theor. Comput. Fluid Dyn.* **10**, 295 (1998).
- ³D. H. Peregrine, "Large-scale vorticity generation by breakers in shallow and deep water," *Eur. J. Mech. B/Fluids* **18**, 403 (1999).
- ⁴O. Bühler, "On the vorticity transport due to dissipating or breaking waves in shallow-water flow," *J. Fluid Mech.* **407**, 235 (2000).
- ⁵A. Piattella, M. Brocchini, and A. Mancinelli, "Topographically-controlled, breaking wave-induced macrovortices. Part 3. The mixing features," *J. Fluid Mech.* **559**, 81 (2006).
- ⁶M. Brocchini, A. Kennedy, L. Soldini, and A. Mancinelli, "Topographically controlled, breaking-wave-induced macrovortices. Part 1. Widely separated breakwaters," *J. Fluid Mech.* **507**, 289 (2004).
- ⁷A. B. Kennedy, M. Brocchini, L. Soldini, and E. Gutierrez, "Topographically-controlled, breaking wave-induced macrovortices. Part 2. Changing geometries," *J. Fluid Mech.* **559**, 57 (2006).
- ⁸U. Putrevu and I. A. Svendsen, "Three-dimensional dispersion of momentum in wave-induced nearshore currents," *Eur. J. Mech. B/Fluids* **18**, 409 (1999).
- ⁹I. A. Svendsen, K. Haas, and Q. Zhao, "Quasi-3D near shore circulation model SHORECIRC, C.A.C.R., Internal Report No. CACR-02-01, University of Delaware, Newark, Delaware (2002).
- ¹⁰Q. Chen, R. A. Dalrymple, J. T. Kirby, A. B. Kennedy, and M. C. Haller, "Boussinesq modeling of a rip current system," *J. Geophys. Res.* **104**, 20617 (1999).
- ¹¹Q. Chen, J. T. Kirby, R. A. Dalrymple, F. Shi, and E. B. Thornton, "Boussinesq modeling of longshore currents," *J. Geophys. Res.* **108**, 3362 (2003).
- ¹²K. Haas and I. Svendsen, "Three-dimensional modelling of rip current systems," Research Report No. CACR-00-06, C.A.C.R., University of Delaware, Newark, Delaware (2000).
- ¹³Q. Zhao, I. A. Svendsen, and K. Haas, "Three-dimensional effects in shear waves," *J. Geophys. Res.* **108**, 3270 (2003).
- ¹⁴J. T. Kirby, Q. Chen, J. Noyes, S. Elgar, and R. T. Guza, "Evaluating the low frequency predictions of a Boussinesq wave model: Field cases," Proceedings of the ISOPE, Honolulu (2003).
- ¹⁵M. Roberts and D. Marshall, "Do we require adiabatic dissipation schemes in eddy resolving ocean models?" *J. Phys. Oceanogr.* **28**, 2050 (1998).
- ¹⁶S. M. Griffies and R. W. Hallberg, "Biharmonic friction with a Smagorinsky-like viscosity for use in large-scale eddy-permitting ocean models," *Mon. Weather Rev.* **128**, 2935 (2000).
- ¹⁷R. Aris, *Vectors, Tensors and the Basic Equations of the Fluid Mechanics* (Dover, New York, 1962), p. 286.
- ¹⁸G. K. Batchelor, *An Introduction to Fluid Dynamics* (Cambridge University Press, Cambridge, 1967), pp. xviii+615pp.
- ¹⁹R. H. Kraichnan, "Inertial ranges in two-dimensional turbulence," *Phys. Fluids* **10**, 1417 (1967).
- ²⁰M. Lesieur, *Turbulence in Fluids* (Kluwer Academic, Dordrecht, 1990), p. 412.
- ²¹C. Schär and R. B. Smith, "Shallow-water flow past isolated topography. Part I. Vorticity production and wake formation," *J. Atmos. Sci.* **50**, 1373 (1993).
- ²²O. Nwogu, "Alternative form of the Boussinesq equation for nearshore wave propagation," *J. Waterway, Port, Coastal, Ocean Eng.* **119**, 618 (1993).
- ²³G. Wei, J. T. Kirby, S. T. Grilli, and R. Subramanya, "A fully nonlinear Boussinesq model for surface waves. I. Highly nonlinear, unsteady waves," *J. Fluid Mech.* **294**, 71 (1995).
- ²⁴A. B. Kennedy, Q. Chen, J. T. Kirby, and R. A. Dalrymple, "Boussinesq modeling of wave transformation, breaking and runup. I. One dimension," *J. Waterway, Port, Coastal, Ocean Eng.* **126**, 39 (2000).
- ²⁵D. Johnson and C. Pattiaratchi, "Boussinesq modelling of transient rip currents," *Coastal Eng.* **53**, 419 (2006).
- ²⁶J. T. Kirby and R. A. Dalrymple, "Modeling waves in surfzones and around islands," *J. Waterway, Port, Coastal, Ocean Eng.* **112**, 78 (1986).
- ²⁷W. R. Dally, R. G. Dean, and R. A. Dalrymple, "Wave height variations across beaches of arbitrary profile," *J. Geophys. Res.* **90**, 11917 (1985).
- ²⁸A. VanDongeren and I. A. Svendsen, "Quasi-3D modeling of nearshore hydrodynamics," Center for Applied Coastal Research, University of Delaware, Internal Report No. CACR-97-04, Newark, Delaware (1997).
- ²⁹C. C. Mei, *The Applied Dynamics of Ocean Surface Waves* (World Scientific, Singapore, 1989), p. 740.
- ³⁰H. T. Özkan-Haller and J. T. Kirby, "Nonlinear evolution of shear instabilities of the longshore current: A comparison of observations and computations," *J. Geophys. Res.* **104**, 25953 (1999).